Timing of Volcanism in Central Oregon: Dating Tam McArthur Rim Volcano

by
Katherine Landoni

A THESIS

submitted to

Oregon State University

Honors College

in partial fulfillment of
the requirements for the
degree of

Honors Baccalaureate of Science in Earth Sciences with a concentration in Geology
(Honors Scholar)

Honors Baccalaureate of Science in Environmental Sciences
(Honors Scholar)

Presented May 31, 2019
Commencement June 2019

# AN ABSTRACT OF THE THESIS OF

Katherine Landoni for the degree of <u>Honors Baccalaureate of Science in Earth Sciences with a concentration in Geology</u> and <u>Honors Baccalaureate of Science in Environmental Sciences</u> presented on May 31, 2019.  Title: <u>Timing of Volcanism in Central Oregon: Dating Tam McArthur Rim Volcano.</u>

Abstract approved:_____

<div align="center">Adam Kent</div>

The Tam McArthur Rim is a volcanic center located within the Tumalo Volcanic Field (TVF), approximately 25 km west of Bend, OR. The rim comprises of shallowly dipping bedded sequences of intermediate and silicic flows with minor tephra interbedding capped by a rhyodacite dome. Glacial activity has exposed significant portions of the flow stratigraphy.

In this study we present new geochronology, petrography, mineral chemistry, and whole rock geochemistry of lava flows from the Tam McArthur Rim. Flow compositions vary significantly, ranging from basaltic andesites to trachyrhyolites. Some flows are aphyric with trachytic flow textures while others are crystal rich, lacking flow textures. Bulk rock geochemistry indicates that these rocks follow a more tholeiitic differentiation trend than typical arc rocks, implying the melt mechanism is not primarily from the introduction of water. Tholeiitic rocks in this geologic setting, like the High Lava Plains of Oregon, are likely due to corner flow of the mantle along the subducting Juan de Fuca plate slab causing decompression melting.

We provide new $^{40}$Ar/$^{39}$Ar geochronology which shows lower portions of the rim are ~185 ka, suggesting volcanism is younger than a previous K-Ar age. The new age data also suggest the Tam McArthur edifice was constructed relatively

quickly, likely within a ~10 ka period. Constraining the timing of past volcanism associated with the TVF provides insights into potential future hazards, allowing for awareness and implementation of informed hazard mitigation strategies within Central Oregon communities.

Corresponding e-mail address: Landonik@oregonstate.edu

Timing of Volcanism in Central Oregon: Dating Tam McArthur Rim Volcano


by
Katherine Landoni




A THESIS


submitted to


Oregon State University

Honors College




in partial fulfillment of
the requirements for the
degree of


Honors Baccalaureate of Science in Earth Sciences with a concentration in Geology
(Honors Scholar)

Honors Baccalaureate of Science in Environmental Sciences
(Honors Scholar)




Presented May 31, 2019
Commencement June 2019

<u>Honors Baccalaureate of Science in Earth Sciences: Geology</u> and <u>Honors Baccalaureate of Science in Environmental Science</u> project of Katherine Landoni presented on May 31, 2019.


APPROVED:


_____

Adam Kent, Mentor, representing Geology Department


_____

Robert Duncan, Committee Member, representing Geology Department


_____

Nicole Rocco, Committee Member, representing Geology Department


_____

Toni Doolen, Dean, Oregon State University Honors College


I understand that my project will become part of the permanent collection of Oregon State University, Honors College.  My signature below authorizes release of my project to any reader upon request.


_____

Katherine Landoni, Author

Table of Contents

# Preface

## Womxn in Geosciences

*Womxn used in this context includes people who are non-binary and women of color.

According to an AGU news report (Wendel, 2015), about 40% of undergraduates in geology are female. However, there is a dramatic decrease in post-academic careers, mostly occurring during choice of undergraduate major and then between PhD and an academic position (figure i) (Holmes et al., 2008). Oregon State University's geosciences program is no different. Womxn[1] are abundant in the undergraduate and even graduate communities. However, faculty is male dominated. According to Wendel, this dichotomy could be due to a time lag where womxn have not yet filtered into higher academic roles. We cannot expect to see parity until "...every geoscience student can see someone on the faculty whose life they wish to emulate" (Wendel, 2015). I will be discussing mentorship and my experiences at Oregon State University as an undergraduate female in Geology.
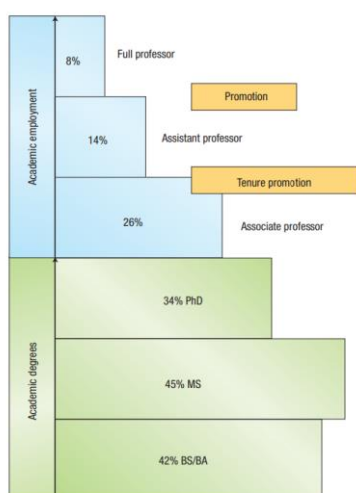


*Figure i: Proportions of women in each academic rank of geosciences from the United States. Although the drop-off between the MS degree and PhD may reflect time lag, the drop off between PhD and assistant professor is real. Figure from (Holmes et al. 2008). Although this figure is relatively outdated, based on Wendel's interpretation, we still see a steep drop off of women in geosciences academic careers after undergraduate.*

Mentoring female undergraduates is crucial for their success. Mentoring provides a window into the culture and norms of geosciences that may otherwise feel foreign. As a female undergraduate it is difficult to feel representation or discover appropriate role models when very few exist, especially those who emulate the life I wish to lead (Wendel, 2015). Although I had a hard time finding mentors who emulate the life I could someday lead in terms of faculty, I have been fortunate enough to find role models in

another place, the geosciences graduate student community. I was paired with Jade Bowers in 2017 and Nicole Rocco in 2018 for the Academic Mentoring Program (AMP) through the College of Earth, Ocean, and Atmospheric Sciences (CEOAS). On the surface, this program matches an undergraduate with a graduate for a term so the undergraduate can gain knowledge about graduate school. Ultimately though, on a deeper level, the AMP program helped me kindle a relationship with a graduate student. Informally, womxn graduate teaching assistants have bolstered the mentorship from the graduate student community.  These womxn graduate students have had big shoes to fill. By mentoring myself and other womxn undergraduates they potentially took on a load that their male counterparts did not.

From my general experience at Oregon State University, I have observed that womxn in CEOAS create a different atmosphere and community than men do. I have some anecdotes regarding how womxn provide a different community.  I found, for example, that when I was taking a lab course, womxn teaching assistants were never purposefully trying to stump me. Instead, I would leave lab feeling as though the teaching assistant was rooting for me by showing excitement and providing resources as I learned new material.

Conversely, the lack of womxn in the laboratory settings was particularly challenging for me and proved to be a significant hurdle; admittedly, more of a hurdle than I was expecting. Most of the mineral preparation rooms and laboratories are predominantly run by men. I find that, broadly speaking, womxn take the time to explain *why* things work whereas men tend to just show *how* things work on a procedural level. My personal learning style relies heavily on the *why*, so I find learning laboratory techniques from womxn to be particularly helpful. Even if the womxn graduate students are not experts, I almost always feel more comfortable going to them for questions. In the laboratory settings I have worked in at Oregon State University, I felt out of place as a female and was definitely a minority.

A final anecdote on how womxn create a different atmosphere from my perspective at CEOAS is in regards to the course "Advanced Field Geology" (GEO 495), colloquially known as "big field camp". Field camp held some of the best and worst

moments of my academic career thus far. I learned how to map under the brilliant, compassionate professor, John Dilles, who was aided by wonderful teaching assistants. I felt strong and empowered with the small group of womxn that I worked closely with as we made observations and conclusions about geologically complex areas. However, there were also some particularly challenging experiences. Several of my bright, younger womxn friends mentioned above and I were discriminated against more than I would have ever anticipated. We were doing particularly well on maps, cross-sections, and descriptions. Our cohort at field camp was dominated by older, ex-military males who had significantly different outlooks than we do. Some of these men found out that the younger womxn were receiving better grades on maps and assignments than they were. From that point forward we were verbally harassed, and our decisions about traverse objectives in the field were nullified. Oregon State brought no womxn teaching assistants. Fortunately, my small group of womxn was supportive and, despite the hardships, we gained so much from the academic and social experiences at field camp.

It would have been a disservice to my undergraduate degree to not include a section in my undergraduate thesis on womxn in geosciences because it has been such an integral part of my experience. Undergraduate womxn need more womxn mentors, period. Womxn graduate students take on this responsibility, but need help. This starts by hiring more womxn into upper-level academic positions. Let's start the dialogue about bringing more womxn, people of color, and LGBTQ+ people to geosciences. Not only do we want to create this dialogue, but we need to raise their voices and listen to them. My experiences as a womxn in geosciences have not made me cynical, but have rather have stoked my fire to incite change.

## References for Womxn in Geosciences

Holmes, M. A., Oconnell, S., Frey, C., & Ongley, L. (2008). Gender imbalance in US geoscience academia. Nature Geoscience, 1(2), 79-82. doi:10.1038/ngeo113

Wendel, J. (2015), Working toward gender parity in the geosciences, Eos, 96, doi:10.1029/ 2015EO031573. Published on 17 June 2015.

## Introduction

The Cascadia subduction zone on the West Coast of North America produces variable volcanism. The relatively young active volcanism in the Central Oregon segment is of particular interest because communities are nearby that are susceptible to volcanic hazards. The Three Sisters and Tumalo Volcanic Field, among other systems, present potential hazards to Bend, Sisters and other towns in Central Oregon. A key part of assessing hazards is understanding the ages and eruptive types of existing volcanism, but the high density of eruptive centers in Central Oregon means that there are many volcanic centers that have relatively poor age control. This study focuses on Tam McArthur Rim Volcano - a small shield volcano located northeast of Broken Top and South Sister. Dating Tam McArthur Rim Volcano provides crucial geochronological data that constrains timing of volcanism in this portion of the Central Oregon Cascades. Understanding timing of volcanism has implications for hazard planning in the communities of Central Oregon including Bend, a population center home to 95,000 people. Characterizing the timing of the Central Oregon volcanic activity is important in planning infrastructure and for community preparedness for volcanic hazards.
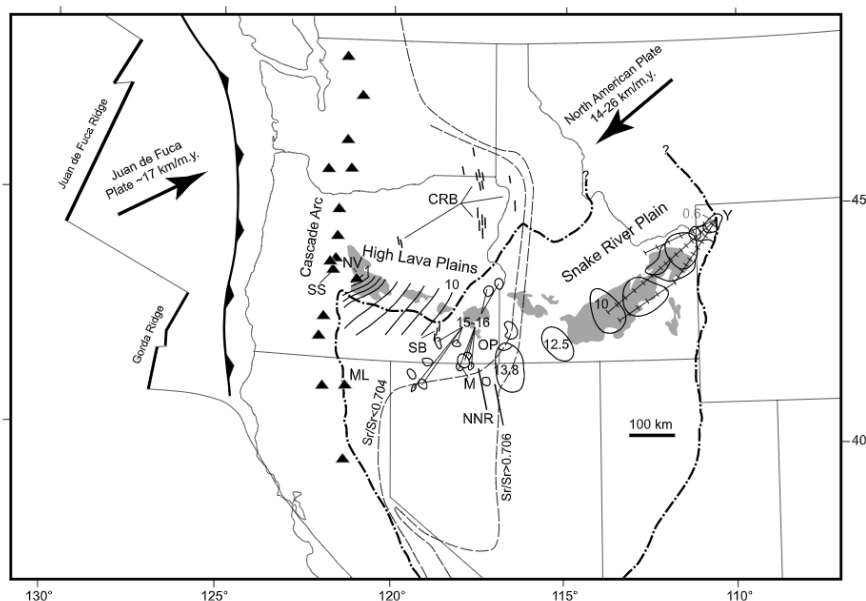


Figure 1: Regional map of the Cascade Arc and High Lava Plains (Jordan et al., 2004).

Some research exists on Tam McArthur Rim, but it is not extensive. Edward Taylor mapped this region in the late 1970's (figure 2) and continued research in the Tumalo Volcanic Field to understand eruptive history (Taylor, 1990). Brittain Hill continued Taylor's work for his dissertation at Oregon State University by acquiring geochemistry and ages for Tam McArthur Rim and surrounding areas (Hill, 1990, and Hill, 1991). In Hill's dissertation, he suggested volcanism shifted west from the Tumalo Volcanic Field to the Broken Top system and Tam McArthur Rim area from ~380 ka until ~100 ka (figure 3) (Hill, 1991).The Broken Top - Tumalo system rhyolites are from 30% to 50% melting of crustal tonalite from Cenozoic Cascadian arc rock and could not have been produced by fractional crystallization (Hill,1991). These conclusions are based on $^{87}Sr/^{86}Sr$ data and REE depletion observations. During this time, Broken Top system rhyolites did not interact with the Three Sisters System. After ~100 ka the eruptive focus shifted from the Broken Top area, northwest to South Sister (figure 3).

Tam McArthur Rim topography was formed by Late Pleistocene glacial excavation leaving behind glacially carved cirques with steep headwalls currently filled by lakes (Taylor, 1978). The lakes that fill the cirques are Three Creek Lake and Little Three Creek Lake, both recreational destinations. From these lakes, an excellent cross-section of the shallow, local volcano's plumbing can be viewed. A rhyodacite dome rim caps underlying lavas at a height of 2,350m. Feeder dikes and lava flows are exposed below the dome. Previous mapping indicate lavas in the steep cliffs are basaltic andesite lavas, dacite lavas, and dacite dikes (Taylor, 1978).



Figure 2: Geologic map of Tam McArthur Rim (Taylor, 1978)
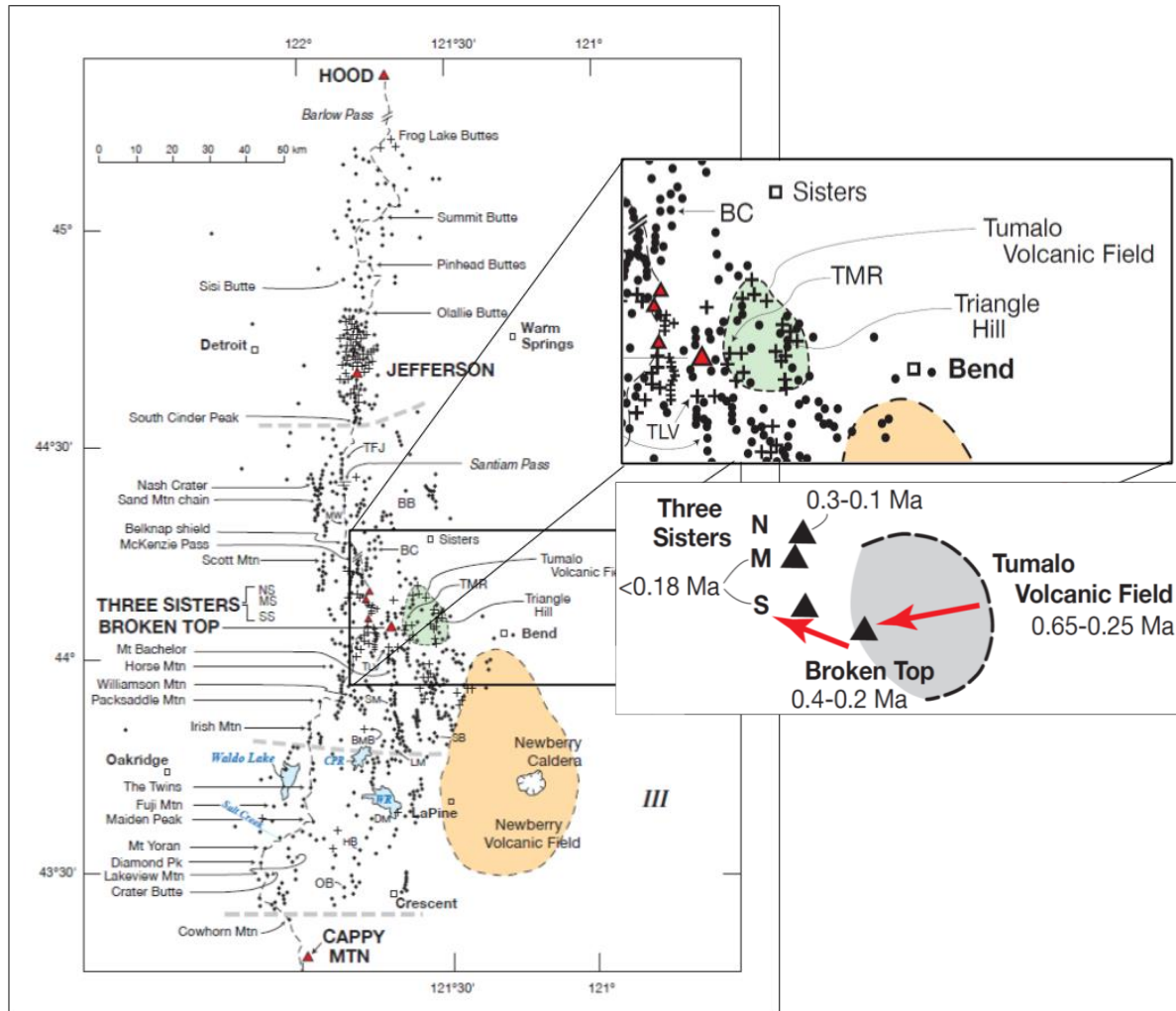
*Figure 3: Regional map of the Central Oregon Cascade arcfront. The insert is of the Broken Top, Tumalo Volcanic Field, and Tam McArthur Rim area. Shifts of eruptive focus from the Tumalo Volcanic Field to South Sister. Dots represent volcanoes of basaltic to andesitic composition; crosses, those of dacitic to rhyolitic composition; and triangles, major edifices. Map adapted from (Hildreth, 2007).*

Currently, there is a single, conventional K-Ar age for the rhyodacite dome at the top of the stratigraphic section at Tam McArthur Rim Volcano. The K-Ar age determined was 213 ± 9 ka (Hill, 1991) and is used to describe relative age relationships with lava from Broken Top's east flank (Sherrod et al., 2004). According to the dome age, Broken Top lavas underlying Tam McArthur Rim volcano were emplaced prior to 213 ± 9 ka (Sherrod et al., 2004). K-Ar ages can be unreliable and less precise because they

potentially do not account for excess argon at time of formation or argon loss during the time the rock has been exposed.

### Objective

This study aims to update the ages for Tam McArthur Rim and underlying units using $^{40}$Ar/$^{39}$Ar geochronology to ultimately aid in refining local stratigraphy. In addition to ages, this study aims to geochemically compare Tam McArthur Rim to nearby systems.

## Analytical Methods

Tam McArthur Rim samples were collected in an attempt to contrast its ages and geochemistry to the nearby volcanism from Broken Top, South Sister, and Tumalo Volcanic Center. All samples were collected by Katherine Landoni and Adam Kent. Samples named "TMR-16-…" were collected in 2016 and samples named "TMR-18-..." were collected in 2018. To further understand the stratigraphy of the excavated volcano, we took panoramic photographs from the cirques, which revealed much of the volcano's stratigraphy.

### Geochemistry

10 whole rock samples were analyzed for major and trace element geochemistry. TMR-16 samples were analyzed at Washington State University and TMR-18 samples were analyzed at Pomona College. These were analyzed using the X-ray fluorescence (XRF) method and trace elements were analyzed using an inductively coupled plasma source mass spectrometer (ICP-MS). This data can be found in the appendix and presented in the results.

### $^{40}$Ar/$^{39}$Ar

A crucial part of this study was to refine the age of Tam McArthur Rim using $^{40}$Ar/$^{39}$Ar geochronology. We selected three samples that characterize Tam McArthur Rim's south end lava flow stratigraphy. These samples are from a lower (TMR-16-01), a middle (TMR-16-02), and an upper (TMR-16-03) stratigraphic flow unit.  I analyzed these three samples utilizing incremental heating $^{40}$Ar/$^{39}$Ar (Koppers, 2002) techniques at Oregon State University's College of Earth, Ocean, and Atmospheric Sciences.

All three samples were analyzed using both Plagioclase and groundmass separates. To create separates, I crushed the hand samples. I sieved, separated, and cleaned the smaller size fractions. Plagioclase grain separates were collected by first separating them from magnetic particles using a Frantz. Cleaning samples required an leaching in 1 N $HNO_3$ to remove mild alteration followed by a rinse in water and drying in the oven. These were then leached in 1 N HF for 15 minutes to remove higher alteration rims on the plagioclase. Following leaching, samples were cleaned with deionized water in an ultrasonic bath and then thoroughly rinsed with deionized water. Finally, these were hand picked for purity under a microscope. Groundmass samples were separated by first leaching the samples in an ultrasonic bath in 1 N $HNO_3$ to remove mild alteration followed by a rinse in deionized water and drying in the oven. Next, the groundmass samples were hand picked under a microscope for purity. No HF leaching was used for the ground mass samples. TMR-16-02 did not produce enough pure plagioclase to further irradiate and subsequently date.

The separates of both plagioclase and ground mass, along with age monitors (Fish Canyon Tuff: 28.201 ± 0.133 Ma) were wrapped in copper foil and weighed. Their heights were measured and were sent to Oregon State University's TRIGA experimental reactor for irradiation. After irradiation, the samples were incrementally heated using a Merchantek integrated $CO_2$ laser until 100% of the cumulative $^{39}Ar$ was released. The released Ar was analyzed by a Thermo Scientific Model ARGUS VI multi-collector mass spectrometer. Data was analyzed in the lab using ArArCALC v2.2 (Koppers, 2002).

## Petrographic

Thin sections were prepared and analyzed to understand the textures of the flows at a microscopic scale under a polarizing light microscope. I observed and characterized the textures and compositions. I photographed portions of the thin sections and completed bed scans. I determined different plagioclase size populations to analyze further with the electron microprobe.

## Electron Microprobe

To characterize populations of plagioclase identified petrographically, thin sections were prepared, carbon coated, and cleaned. I acquired backscattered electron images using Oregon State University's Cameca SX-100 Electron Microprobe. To understand compositional stages, I analyzed three plagioclase populations. These three populations are relative (megacrysts, phenocrysts, and microlites) and were analyzed in samples TMR-16-01, TMR-18-04, TMR-18-08, and TMR-18-10. Microlites are defined in this study as small crystals found in the groundmass. Phenocrysts are defined as distinct from the groundmass. Megacrysts are defined as significantly larger than both the microlites and megacrysts.

The electron microprobe was calibrated to analyze plagioclase (i.e. Na, Si, Al, Fe, Ca, K, Mg, Ti, O) using the LABR standards. The beam had a diameter of 5μm with a 30 nA current.

# Results

## Field

The shallow dipping flanks of Tam McArthur Rim are comprised of flows that vary in composition (figure 9) from basaltic andesite to trachyte to rhyodacite at the uppermost dome. Flows vary from ~1 meter up to ~20 meters thick. In some areas flows are difficult to distinguish from each other laterally and commonly pinch out into each other (figure 6). These flows are locally interbedded with at least two thin pyroclastic units, have cross-cutting dikes, and at least one massive obsidian flow that acts as a marker bed. Based Taylor's mapping, this is the same material as the rhyodacite dome. It is refered to in the literature as a black glassy rhyodacite.  In the central portion of the rim, a rhyodacite dome sits above the lava units (figures 9 and 10- point A).
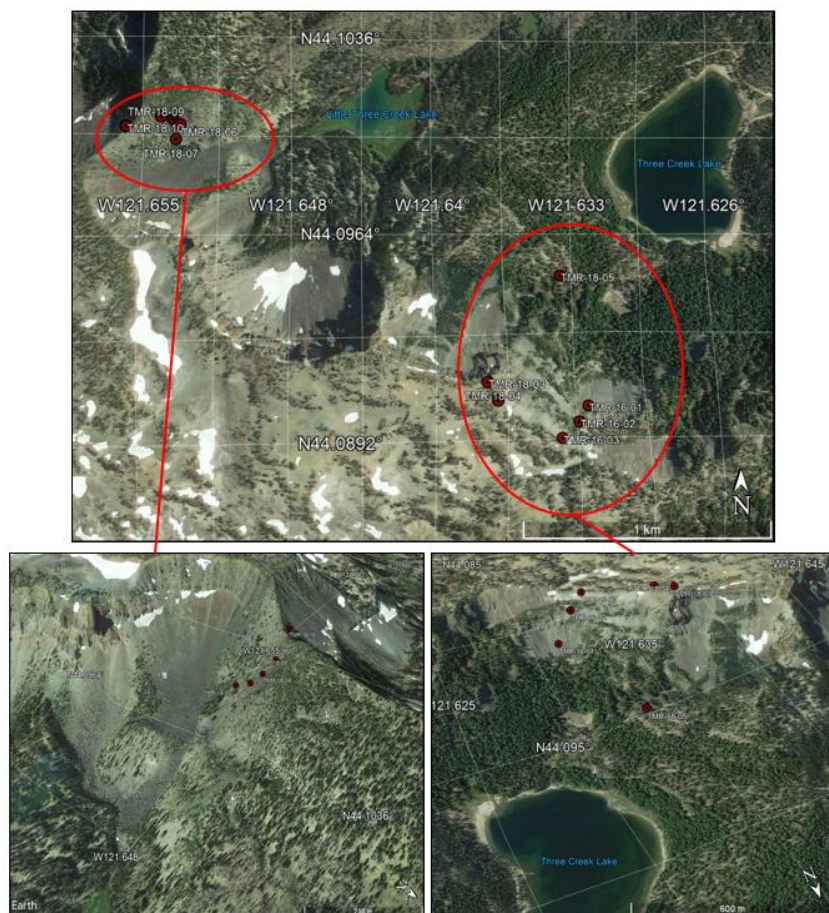
*Figure 4: Google Map plan view of all sample locations (top). Oblique views of sample locations (bottom). See appendix for latitudes, longitudes, and elevations of all samples.*
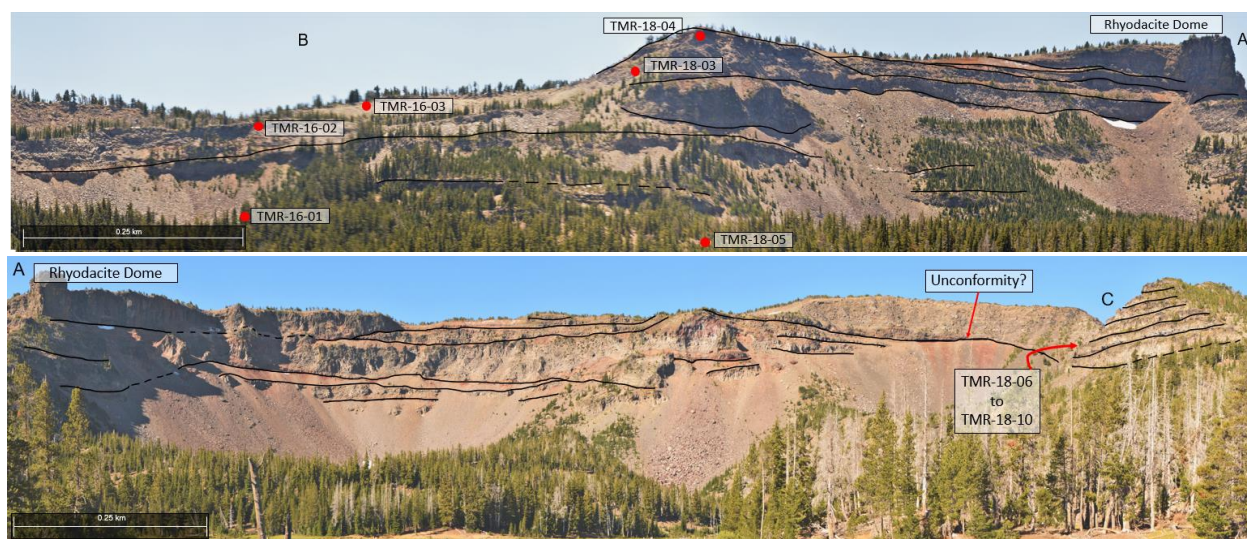
Figure 5: (previous page) Photo from Three Creek Lake (top) at the Southern cirque of TMR. The Rhyodacite dome (A) is at 44° 5' 34.24" N, 121° 38' 36.76" W. To the left are gently dipping flow units where TMR-16-01, TMR-16-02, and TMR-16-03 samples were collected for $^{40}Ar/^{39}Ar$ dating below "B".

Figure 6: (previous page)Photo from Little Three Creek Lake (bottom) of the Northern cirque of the TMR. To the left is the Rhyodacite dome (A), and the terminus of the TMR trail. To the right (C) is 44° 06' 0.14" N, 121° 39' 20.20" W, where the view of the majority of the TMR-18 suite of samples is blocked. Potential unconformity is labeled.
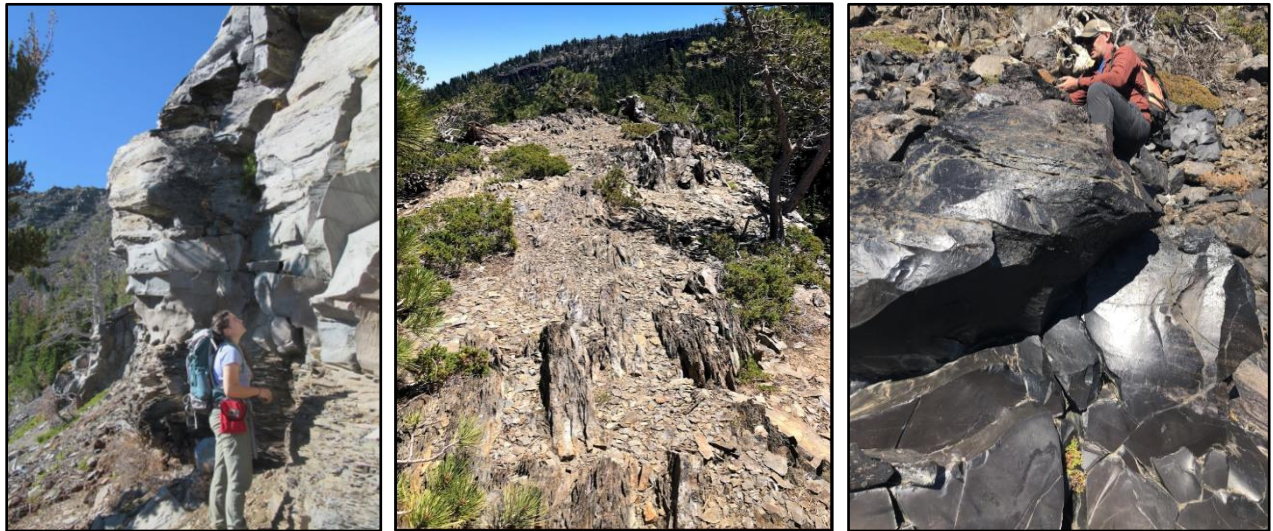


Figure 7: (left) Massive, thick andesite flow about 5 m tall with a horizontal platy basal layer. 1.65m human for scale. Location is C from figure 5. (middle) Horizontal platey fracturing of dike at sample location TMR-18-05 on figure 5. (Right) Massive, 1 meter thick obsidian flow. Location is TMR-18-09 from figure 6.

# [40]Ar/[39]Ar Ages
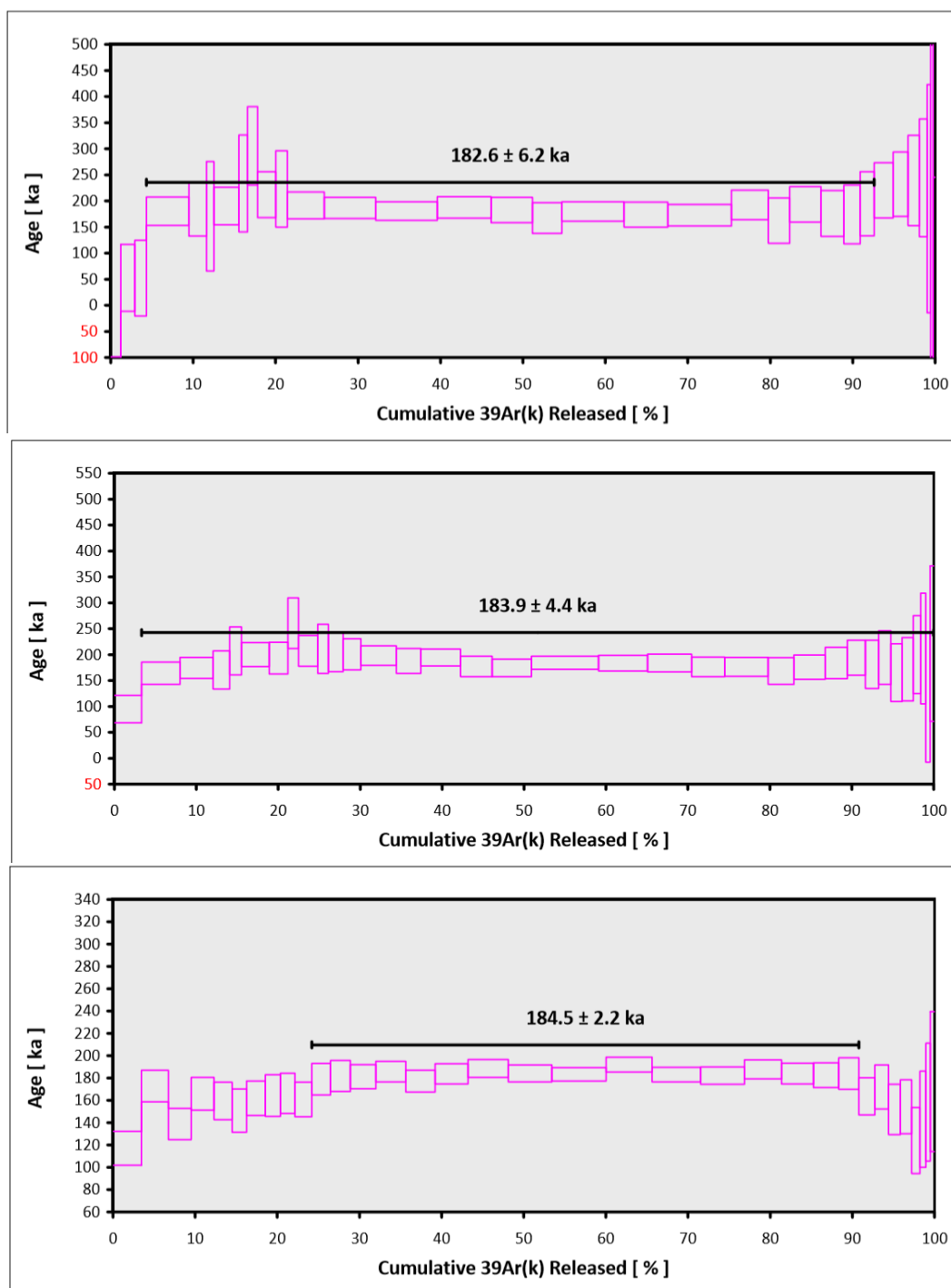


*Figure 8: [40]Ar/[39]Ar ages for TMR-16-01 (bottom), TMR-16-02 (middle), and TMR-16-03 (top). The stacking of these graphs represents their relative location in stratigraphy.*

| Sample ID | Total Fusion (ka) | 2s error (Ka) | Isochron age (Ka) | 2s error (Ka) | MSWD | $^{40}Ar/^{36}Ar$ initial | 2s error |
|---|---|---|---|---|---|---|---|
| TMR 16-03 | 178.6 | ± 7.8 | 176.8 | ± 19.6 | 0.48 | 298.03 | ± 8.34 |
| TMR 16-02 | 182.1 | ± 6.2 ka | 194.2 | ± 13.4 ka | 0.75 | 286.87 | ± 9.36 |
| TMR 16-01 | 174.4 | ± 4.5 ka | 187.9 | ± 19.2 ka | 0.75 | 286.36 | ± 45.35 |

| Sample ID | Plateau age (Ka) | 2s error (Ka) | N | MSWD | Notes |
|---|---|---|---|---|---|
| TMR 16-03 | 182.6 | ± 7.4 ka | 33 | 0.48 | 40Ar loss at lower temperature and recoil in higher release steps. |
| TMR 16-02 | 183.9 | ± 6.0 ka | 34 | 0.85 | 40Ar loss at lowest temperature step and  high point in plateau. |
| TMR 16-01 | 184.5 | ± 4.7 ka | 34 | 0.73 | 40Ar loss at lower temperature steps. |

*Table 1: Total Fusion, Isochron, and Plateau ages and associated errors for groundmass separates from samples TMR-16-01, TMR-16-02, and TMR-16-03.*

## Geochemistry
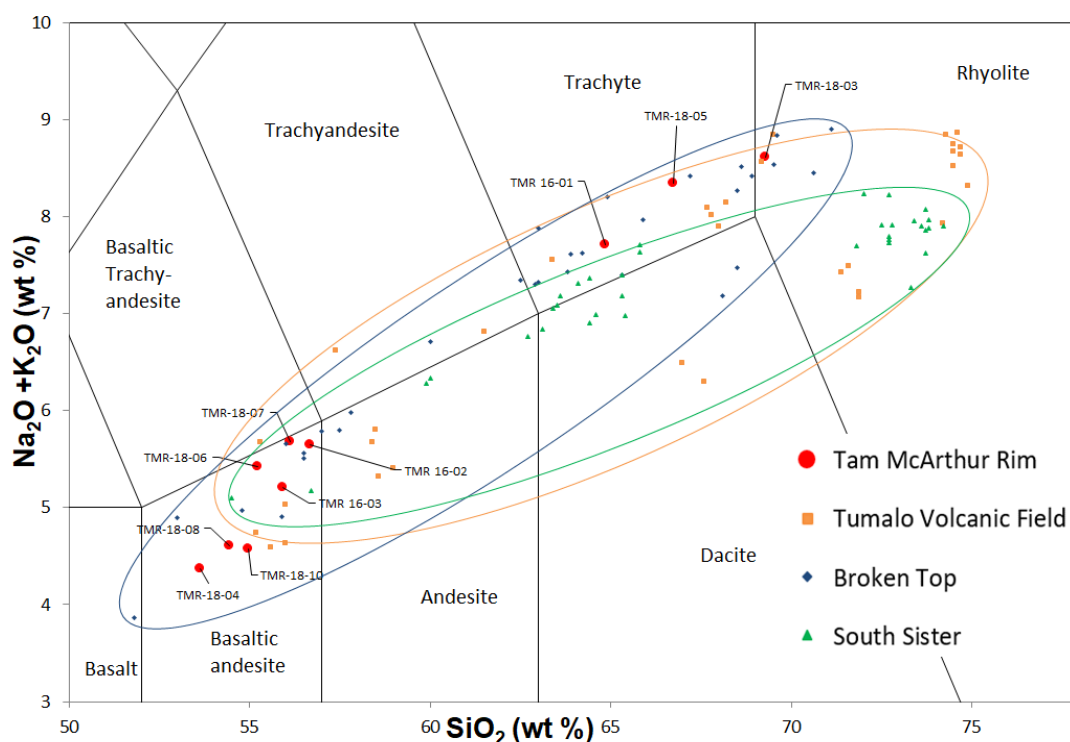


*Figure 9: Total Alkali Silica (TAS) plot shows regional volcanic compositions from South Sister, Broken Top, and Tumalo Volcanic Field. Compositional fields are similar and show that Tam McArthur Rim bulk geochemistry samples follow the regional volcanic compositions, but more closely Broken Top.*
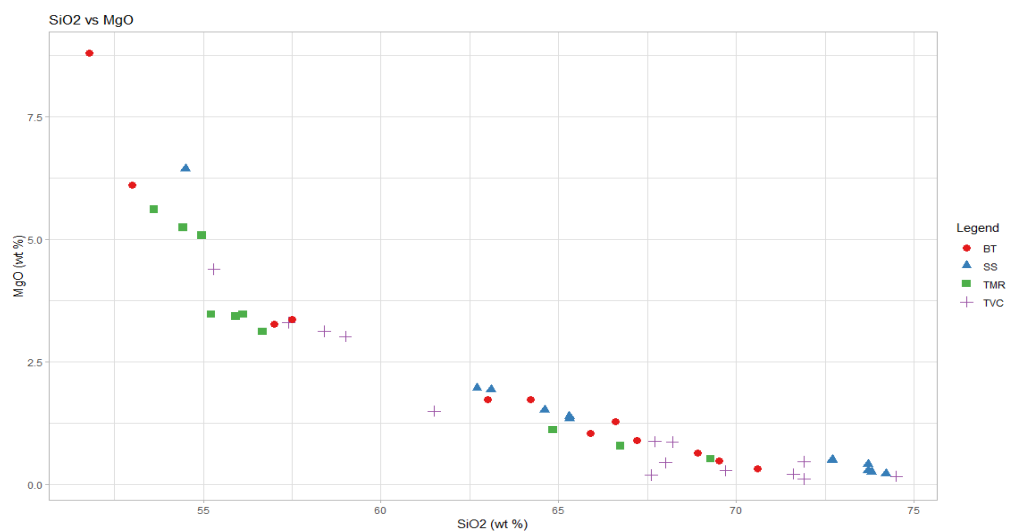
*Figure 10: Harker Plot of SiO$_2$ and MgO of Broken Top (BT), South Sister (SS), Tam McArthur Rim (TMR), and Tumalo Volcanic Center (TVC).*
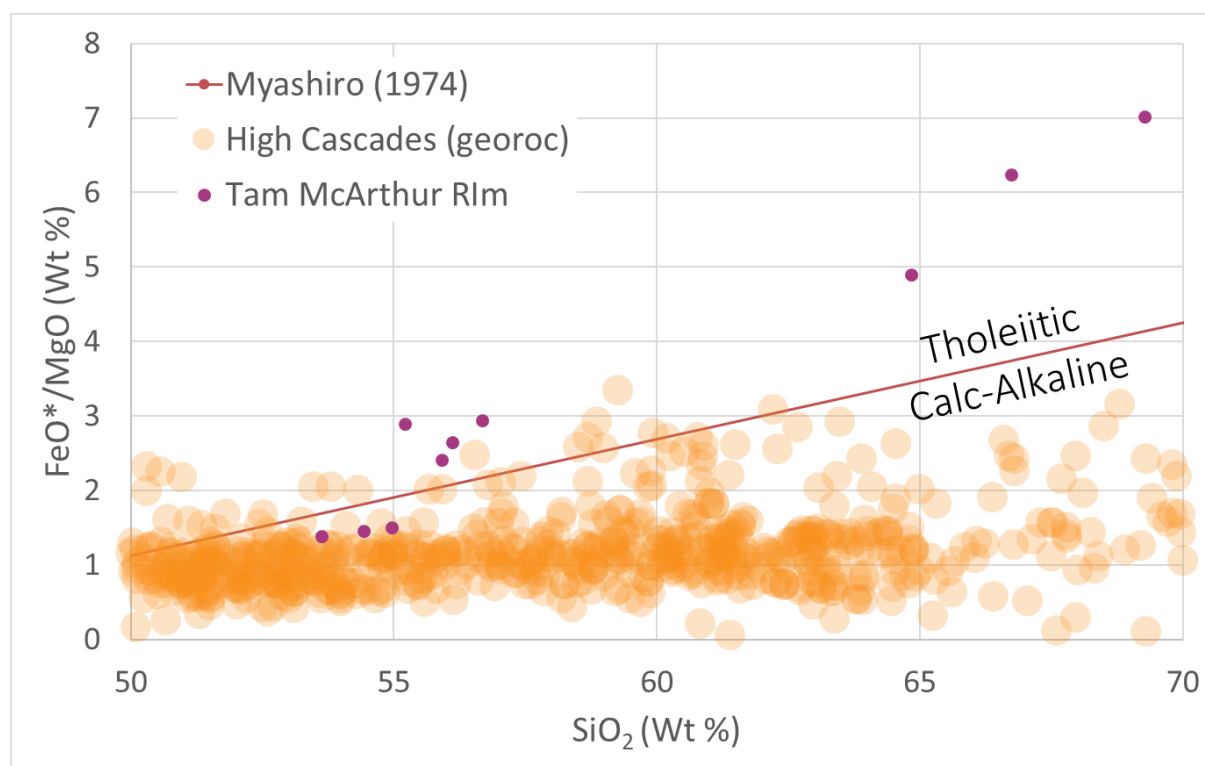


*Figure 11: Tam McArthur Rim lava flows and High Cascades plotted to differentiate between tholeiitic and calc-alkaline determined by Myashiro (1974). Thee points plotting as tholeiitic are from overlying Broken Top lavas.*
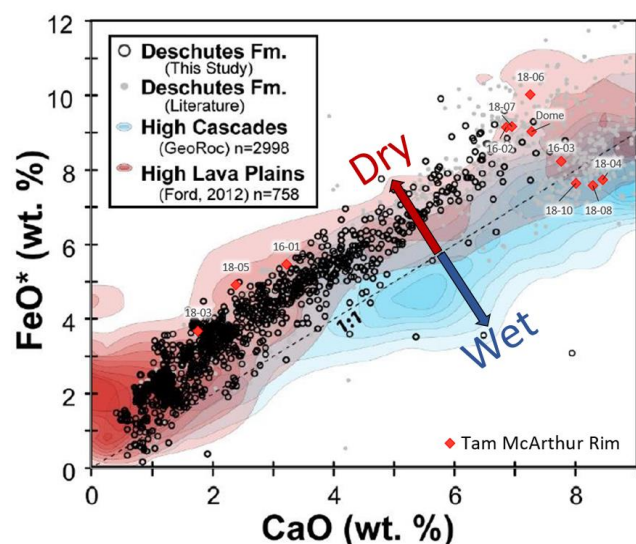
Figure 12: FeO* vs CaO with a dashed line denoting a 1:1 slope. FeO* represents the total for all Fe species. Adapted from (Pitcher, 2017). Tam McArthur Rim lavas for this study plotted along with the rhyodacite dome as red diamonds (Hill & Priest, 1992a).
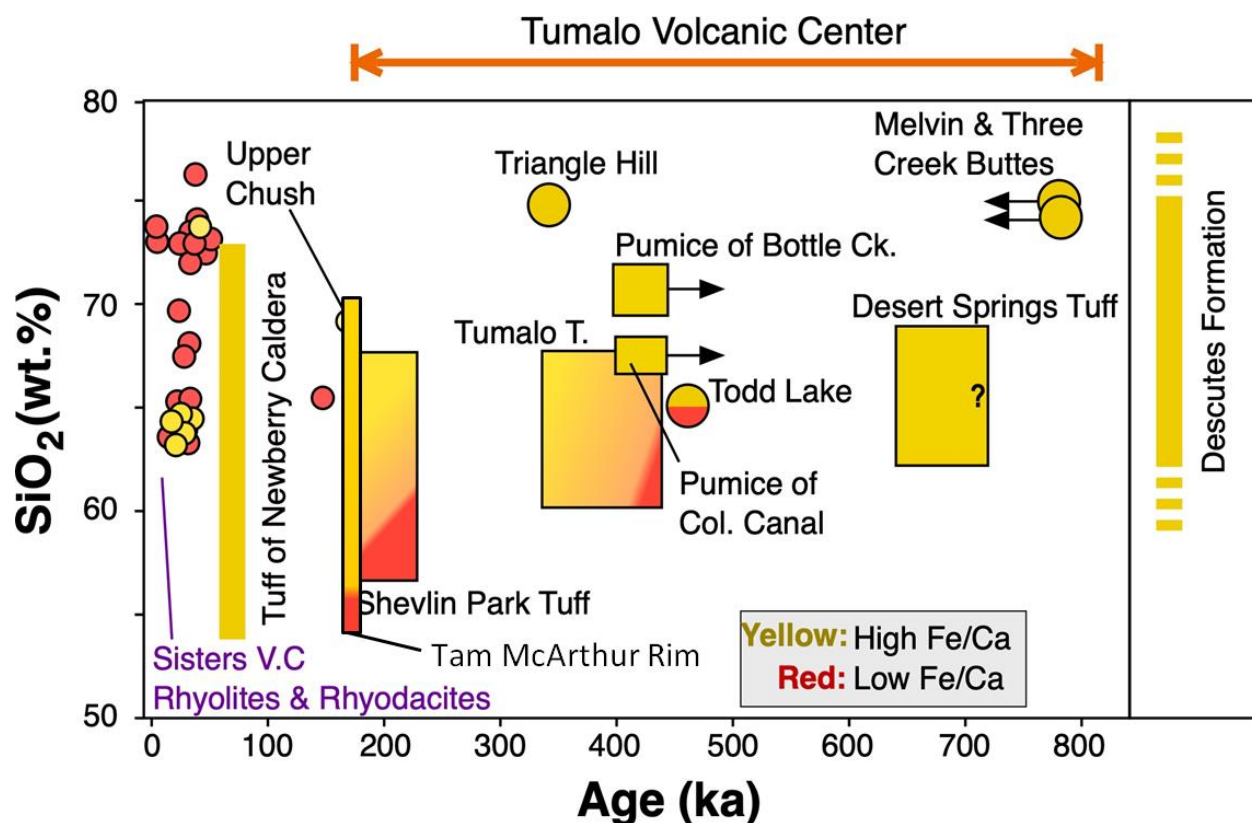


Figure 13: Summary figure of geochemistry and age data. Fe/Ca ratios for the Tumalo Volcanic Center region and other nearby systems are plotted to represent dry (yellow) and wet (red) mamas. Tam McArthur Rim plots over part of the Shevlin Park Tuff. $SiO_2$ increases with increasingly dry magma for the Tam McArthur Rim. Adapted from (Kent, unpublished).

## Petrography

Petrographic analysis was used to characterize the lava flows and served as a precursor to Electron Probe Analysis. Samples fell into two main categories (trachytic and felty).

**TMR-16-01**
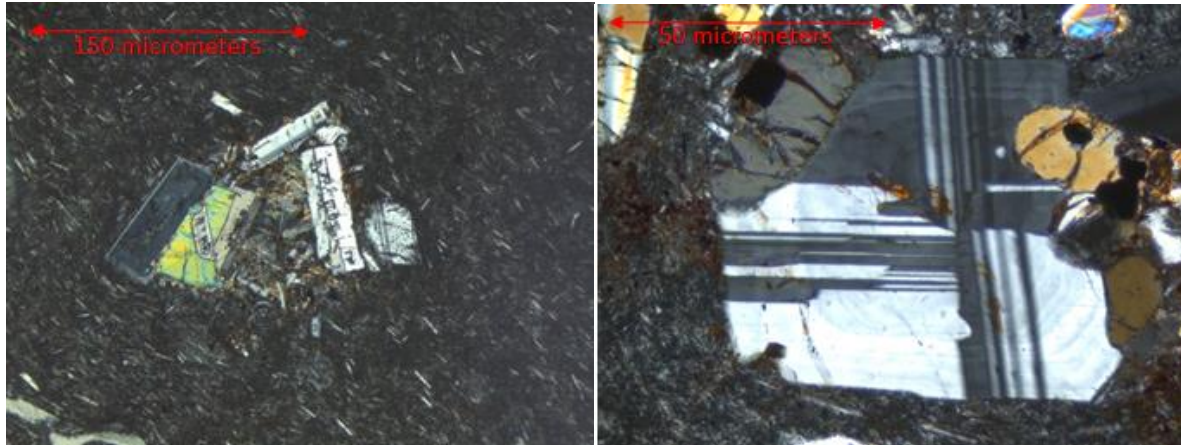


Glomerocrysts were observed and consist of plagioclase, olivine and pyroxenes. Plagioclase crystals show a sieved textures, twinning, and oscillatory zoning. Ground mass has weakly trachytic plagioclase elongate needles and oxides.

---

**TMR-16-02**
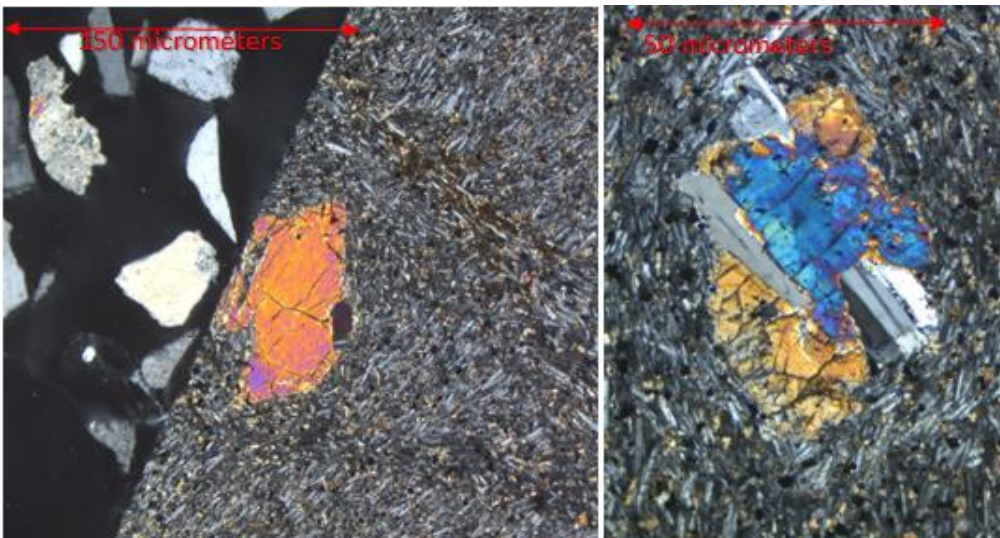


This sample is ~95% ground mass and ~5% crystals. Groundmass has a subophytic, trachytic texture of plagioclase, pyroxenes, and magnetite. Glomerocryst clots of plagioclase, olivine, and pyroxenes. Plagioclase phenocrysts have olliatory zonation, twinning, and sieved textures.

## TMR-16-03
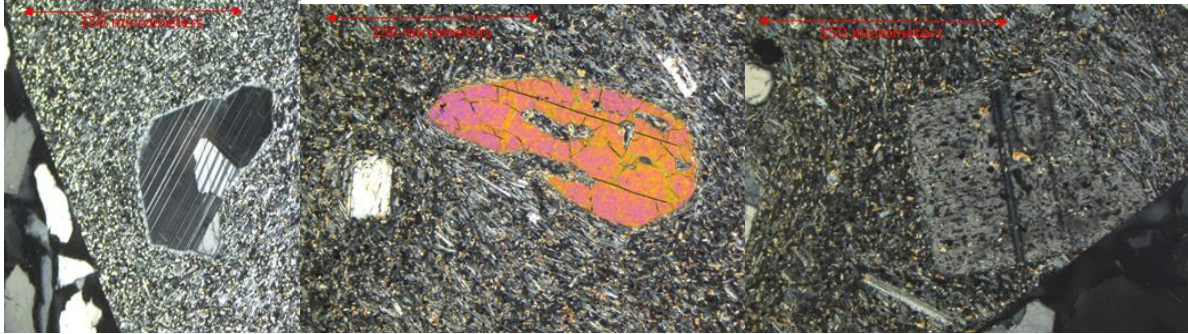


Moderately trachytic groundmass texture is subophytic. Plagioclase phenocrysts range from twinned and euhedral (left), to almost entirely sieved with replacing mineral inclusions (right).

## TMR-18-04



This sample is vesicular, crystal rich, and non-trachytic. It has many different sized phenocrysts from groundmass subophytic microlites to macrocrysts. Glomerocrysts clots (left) are common. Skeletal Olivine (middle) displays a dissolution texture replaced with plagioclase. Plagioclase grains are twinned, sieved, oscillatory zoned, have melt inclusions, and show undulatory extinction. This sample shows more olivine than other samples in this suite.

**TMR-18-05**
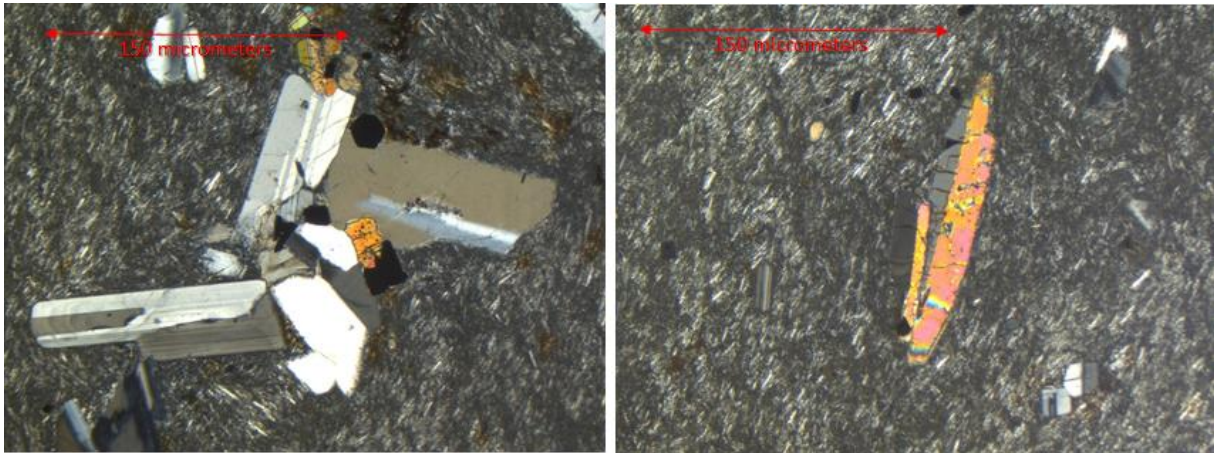


This sample is a porphyritic, moderately trachytic, crystal poor, groundmass dominated sample. Olivine, plagioclase, and orthopyroxenes are present as both glomerocrysts and phenocrysts. This sample was taken from a potential feeder dike.

**TMR-18-06**
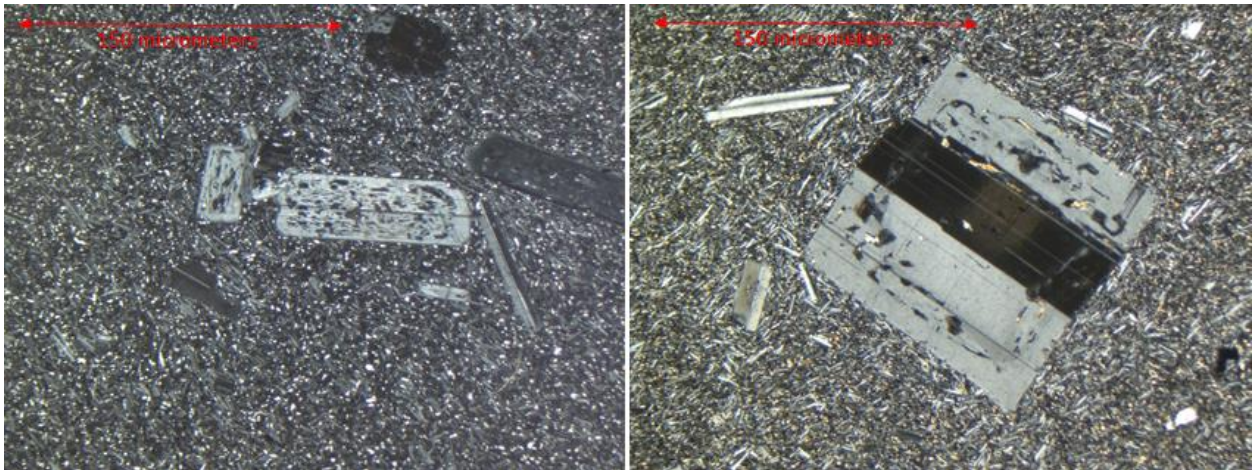


Groundmass dominates this sample and is subophytic with oxides. The phenocrysts are dominantly plagioclase with sieved, zoned, and twinned textures. Some portions show weak trachytic flow textures.

**TMR-18-07**
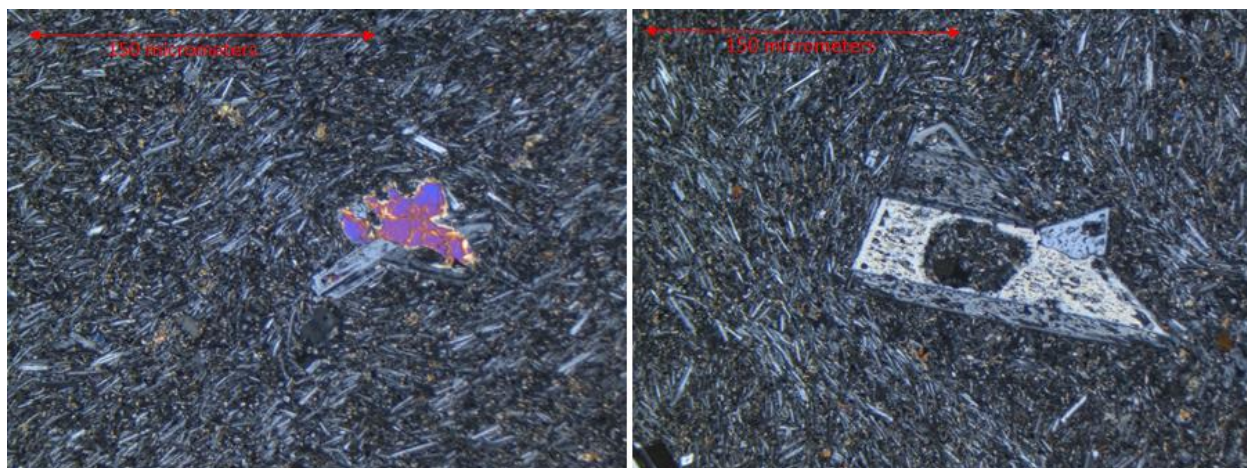


This sample is dominated by an trachytic, subophytic groundmass with oxides and is porphyritic. The phenocrysts compositions are olivine and plagioclase and have sieved and dissolution textures.

---

**TMR-18-08**
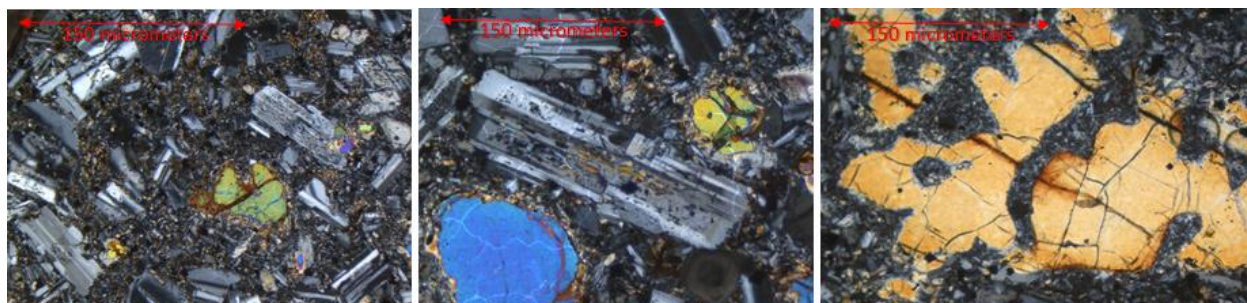


Similar to sample TMR-18-04, 18-08 is crystal rich and not trachytic. Glomerocrysts and phenocrysts  are present. Olivine, orthopyroxenes, and plagioclase are present. However, many crystal show sieved and disequilibrium textures. Dissolution textures are in the center and right photos showing plagioclase and olivine dissolving respectively.

**TMR-18-10**
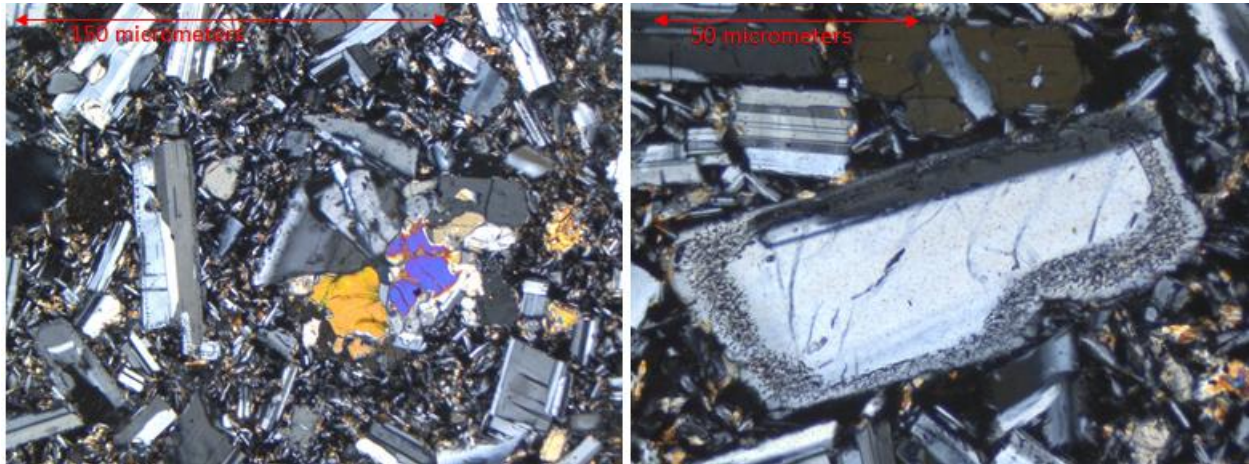


TMR-18-10 is similar to both TMR-18-08 and TMR-18-04. It shows no trachytic flow textures, is crystal rich. The ground mass is subophytic and magnetite groundmass. However, it varies from these sample because its dominant phenocryst is plagioclase. Radial glomerocryst (left) and twinned, plagioclase with sieved texture below the rim.

## Electron Microprobe

Electron Microprobe analysis provided backscatter images and grain compositions. Populations of plagioclase analyzed were microlites, phenocrysts, and megacrysts.
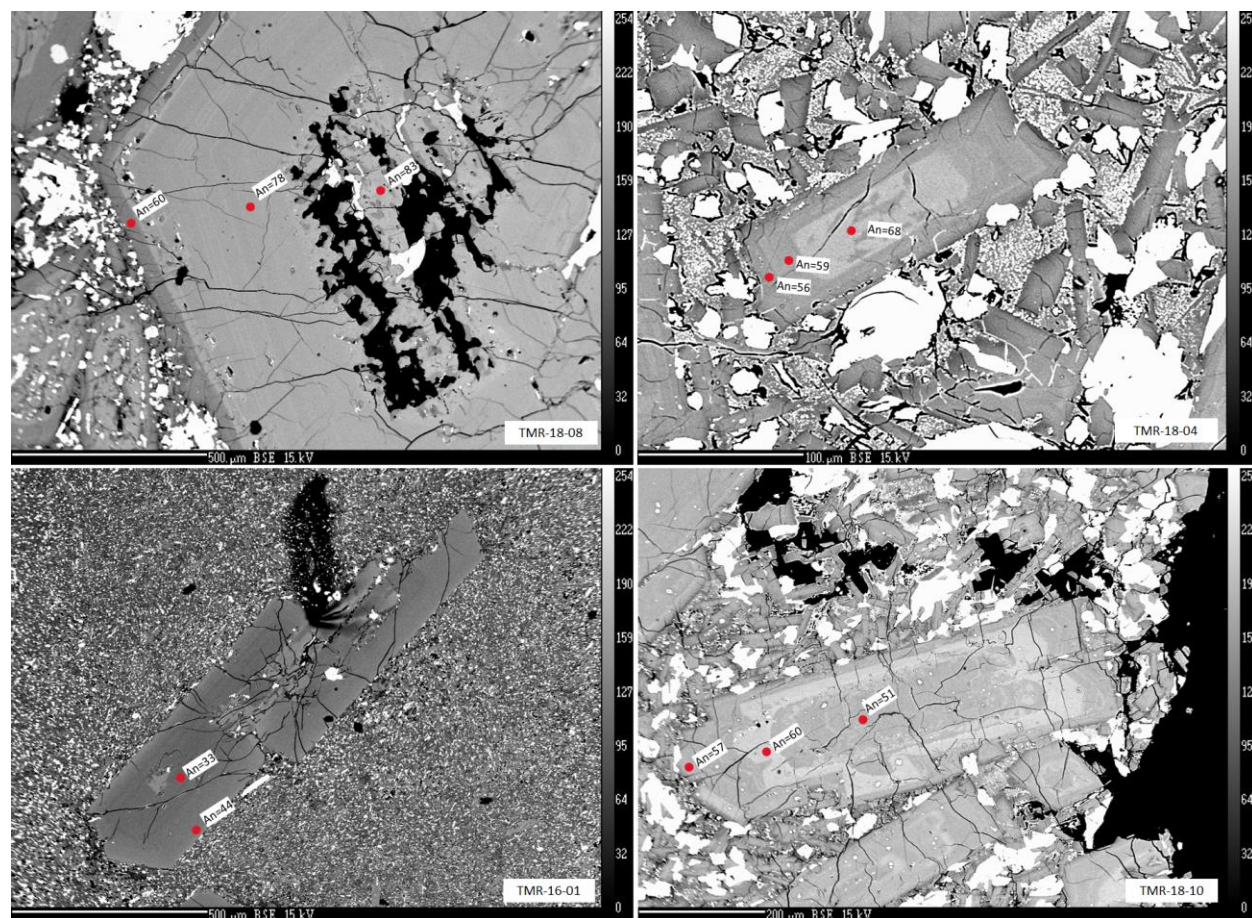


*Figure 14: BSE images.*

*TMR-18-08: (top left) Plagioclase megacryst showing sieved core, some oscillatory zoning, but overall normal zoning. The rims are underlain by a sieved texture.*

*TMR-18-04: (top right) Plagioclase phenocryst  showing normal zoning, surrounded by other plagioclase phenocrysts and microlites.*

*TMR-16-01: (bottom left) Megacryst of plagioclase showing reverse compositional zoning. Groundmass is composed of mostly microlites.*

*TMR-18-10: (bottom right) Megacryst of plagioclase showing oscillatory zoning. Surrounded by phenoycrystic and microlitic plagioclase.*
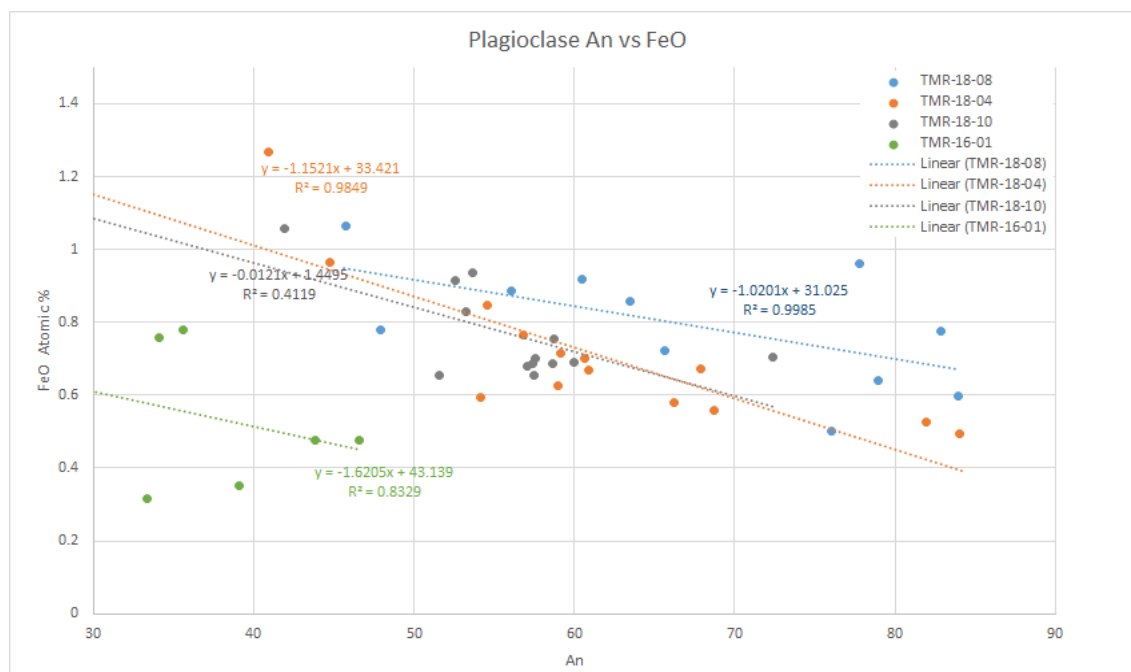
*Figure 15: Plagioclase compositions of An vs FeO (Atomic %) from Electron Microprobe analysis (Appendix B).*
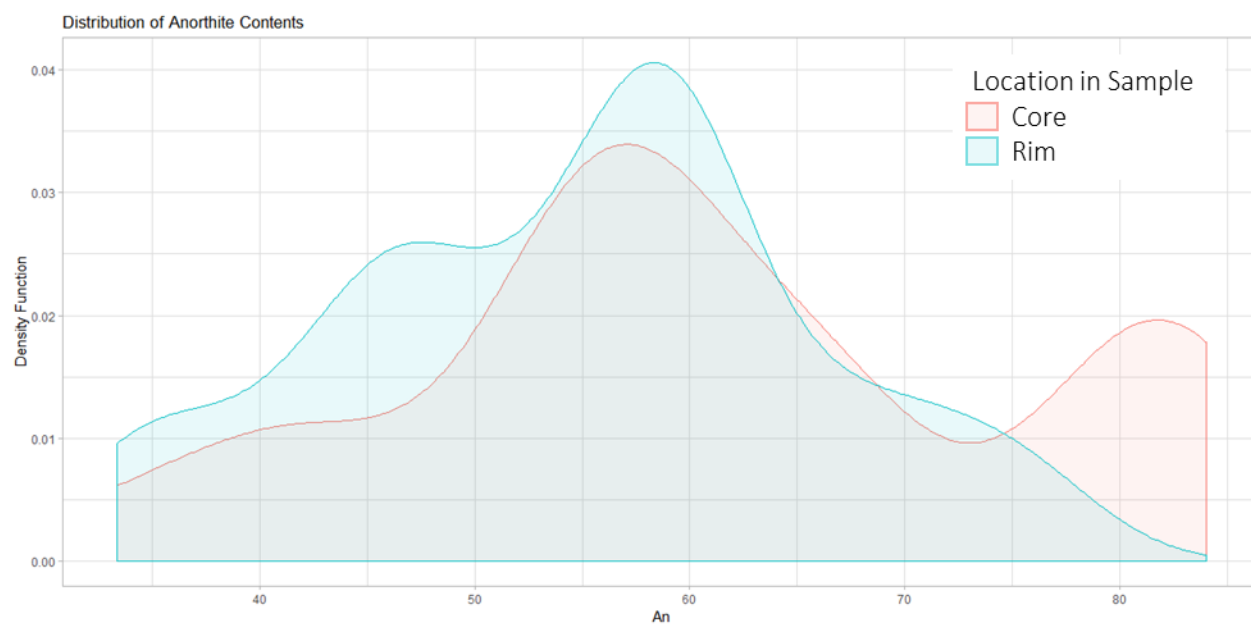


*Figure 16: Distribution of anorthite contents by location in crystal (core vs rim) determined in Electron Microprobe analysis (Appendix B).*
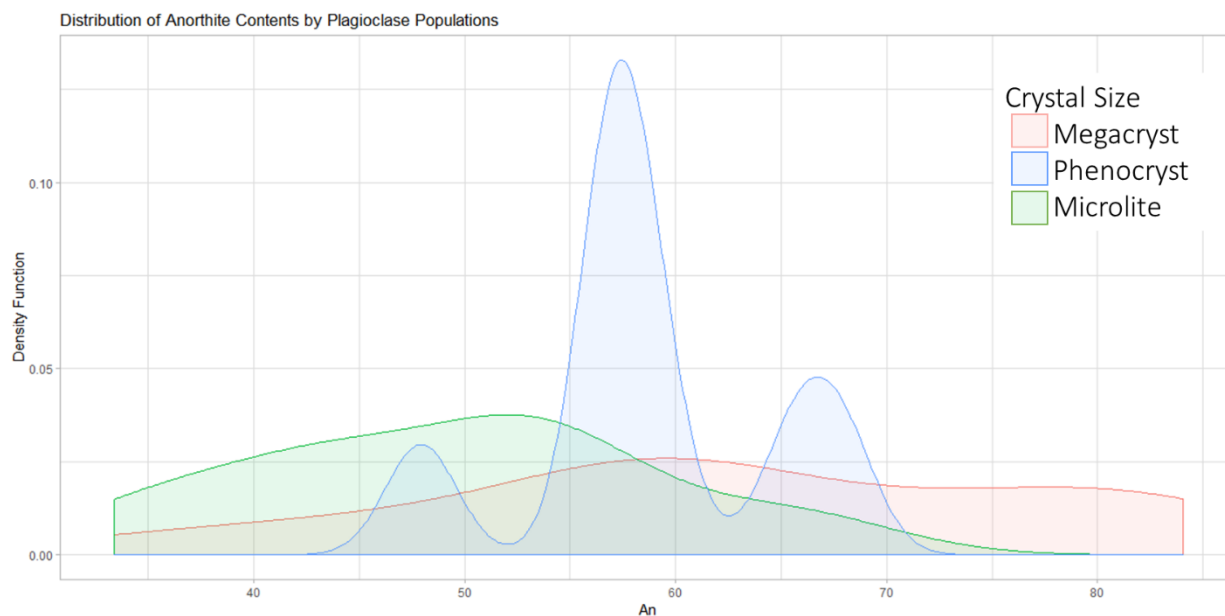
*Figure 17: Distribution of anorthite contents by plagioclase population crystal sizes of megacryst, microcryst, and phenocryst determined by Electron Microprobe analysis (Appendix B).*
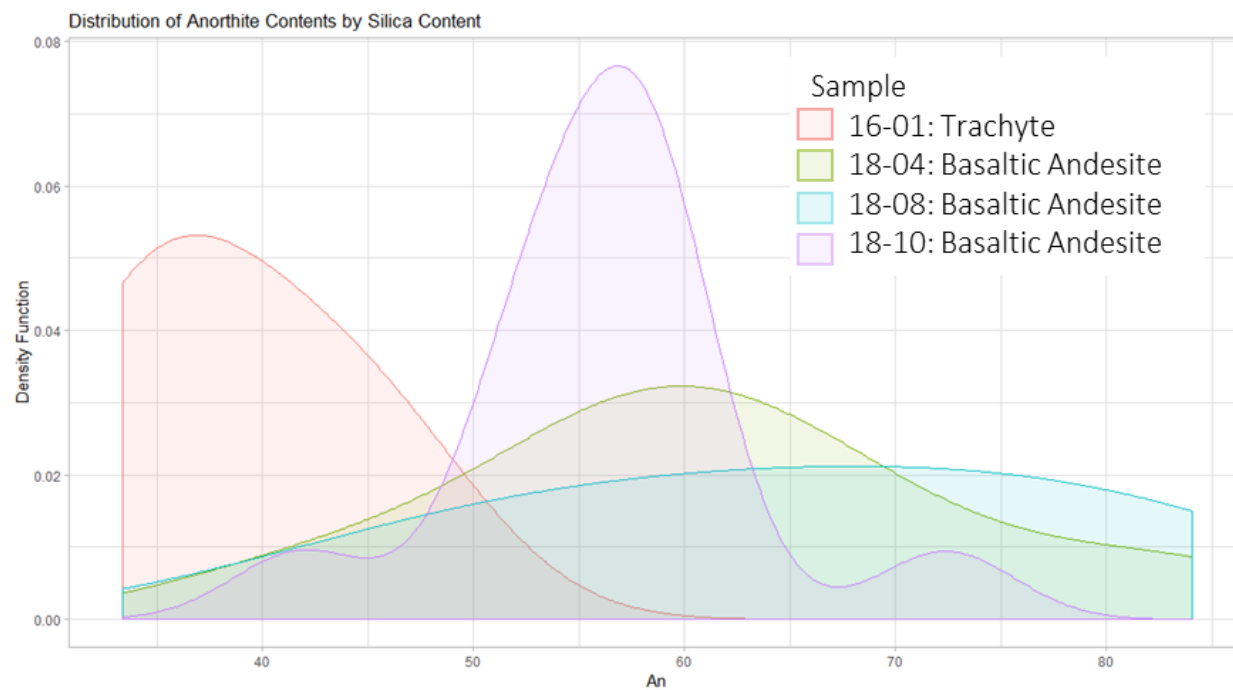


*Figure 18: Distribution of anorthite contents by Silica content determined by microprobe analysis (Appendix B).*

# Discussion

## Field Relations

Tam McArthur Rim is a small shield volcano with shallow dipping lava flows away from the presumed vent area, marked by a rhyodacite dome that sits atop the flow layers. Flows are cut by dikes and are ultimately exposed as glacial cirques due to Late Pleistocene glaciation (Taylor, 1978). Glacial erosion has exposed 300 vertical meters of the shallow plumbing and lava flow stratigraphy of Tam McArthur Rim volcano. The flows range from less than a meter thick to over 20 m thick in some places. Interbedded with the lava flows are at least two thin pyroclastic deposits of unknown origin, and a one meter thick massive obsidian flow. An unconformity was observed in the northwestern cirque (figure 19). Lava flows that overlie this unconformity do not conform to the dip of the flow beds beneath them and are likely Broken Top lavas (Taylor, 1978). Flows directly below the unconformity have developed what appears to be a paleosol that drapes the slopes as a red talus as seen in figure 5 and are likely from Tam McArthur Rim. Future dating will assess the ages of the Broken Top flows above the unconformity (figure 19).
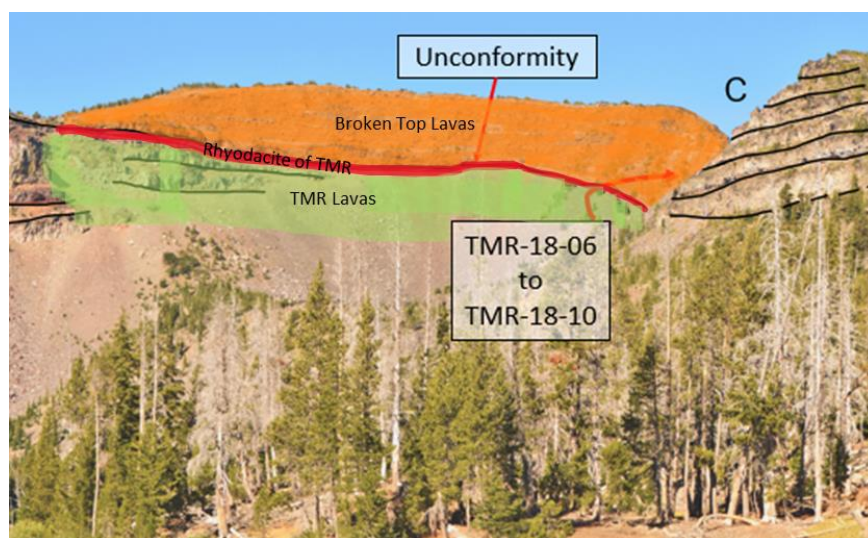


Figure 19: Broken Top lavas overlying the unconformity that represents the youngest Tam McArthur Rim flows.

Samples were obtained on the sloping lava flow flanks, but we did not directly sample the dome or vent area. The sample locations are bimodal, one area to the southeast of the dome, and one to the northwest of the dome. Mapping lava flow units proved to be difficult based on steep topography. The flows are relatively horizontal with a slight dip away from the rhyodacite dome. Many flows were too variable in their thickness and too thin to be mapped as distinguished units.

## Ages

$^{40}$Ar/$^{39}$Ar dating analyses of three units from the southeast flanks of Tam McArthur Rim volcano all corroborate observed stratigraphic field relations. The plateau age from the oldest trachytic flow unit (TMR-16-01) is 184.5 ± 2.2 ka. This sample is the most silicic and alkaline of the dated rocks and is from the bottom of the exposed stratigraphic section, closest to Three Creek Lake. The second sample, a basaltic andesite flow unit (TMR-16-02) has a plateau age of 183.9 ± 4.4 ka is found in the middle of the stratigraphic section. Finally, the youngest basaltic andesite flow unit (TMR-16-03) has a plateau age of 182.6 ± 6.2 ka and is found closest to the rim of the cirque and is part of the upper stratigraphic flow units. This youngest flow, with an age of 182.6 ± 6.2 ka, underlies a rhyodacite dome that has a previously cited K-Ar age of 213 ± 9 ka (Hill, 1991). We did not date the rhyodacite dome, but found that, outside of error, the previous rhyodacite dome K-Ar age is too old.

I propose the dome's age is actually younger than 182.6 ka based on stratigraphic superposition. $^{40}$Ar/$^{39}$Ar dating has provided more better age constraints of the local systems. However, $^{40}$Ar/$^{39}$Ar dating is necessary at the northeastern rim, where the majority of the TMR-18 sample suite was obtained. Redating the dome itself with $^{40}$Ar/$^{39}$Ar analysis could prove fruitful as it could provide a minimum age for Tam McArthur Rim. Additionally, dating the Broken Top flow that overlies the unconformity could help clarify how Tam McArthur Rim volcano is temporally related to Broken Top. Relative to nearby volcanoes, Tam McArthur Rim is on the younger end of the Tumalo Volcanic Center which ranges from about ~150 - ~800 ka (figure 13). However, because Tam McArthur Rim lavas cover the Triangle Hill vent, it is likely that Tam McArthur Rim and other contemporaneous Broken Top lavas are younger than the Tumalo Volcanic Center itself (Hill, 1990). Broken Top was active between ~150 - ~300 ka contemporaneous with Tam McArthur Rim deposits (Hildreth, 2007). Recent eruptions at the Sisters Volcanic Center are significantly younger than Tam McArthur Rim between ~2 - ~50 ka.

## Bulk Rock Geochemistry

Bulk geochemical analyseis of these rocks show a general bimodal distribution. The two rock types are basaltic andesite and trachyte/trachyrhyolite (Figure 9). The three most mafic samples, basaltic andesites, are found stratigraphically highest and likely from Broken Top (TMR-18-04, TMR-18-08, and TMR-18-10). The rest of the samples are all basaltic andesite and trachyte and are found lower in the stratigraphic sequence of lava flows. The remaining samples are thought to be directly from Tam McArthur Rim Volcano. In general, this implies more silicic and alkali rich lavas were erupted first from Tam McArthur Rim Volcano, followed by the more mafic basaltic andesites from Broken Top.

Arc rocks are typically calc-alkaline due to the presence of water during mantle melting and differentiation. We observe that MgO does decrease with increasing $SiO_2$, and follows the same broad trends as Broken Top, South Sister, and the Tumalo Volcanic Field (figure 10). However, a more significant observation is that Tam McArthur Rim compositions follow a sub-tholeiitic differentiation trend, and not calc-alkaline differentiation trend. However, Broken Top, South Sister, and the Tumalo Volcanic Field also show tholeiitic compositions (figure 11).

To investigate this further, I plotted FeO* by CaO to compare them to the High Lava Plains, the High Cascades, and the Deschutes Formation (figure 12) (Pitcher, 2017). Points plotting above the 1:1 line are presumed to have followed a tholeiitic liquid line of descent and are derived from dryer magmas. Points plotting below that 1:1 line are thought follow a calc-alkaline liquid line of descent and are derived from wetter magmas (Miyashiro, 1974). A reducing environment can also produce FeO*/MgO contents that plot in the thoeilitic region (Sisson et al., 2005).

Most Tam McArthur Rim samples, especially the felsic rocks, plot above this 1:1 line. The three most mafic samples, likely from Broken Top, plot below the 1:1 line. The more felsic rocks ($SiO_2$ > 55 wt %) in this study are likely derived from a dryer magma, following a tholeiitic differentiation trend. The more mafic rocks ($SiO_2$ < 55 wt %) may be derived from a wetter magma, following a calc-alkaline differentiation trend, more analogous with typical arc rocks. Lower water in a magma means the magma is in a

reducing state. This means magma to preferentially crystallizes Mg bearing minerals first, initially enriching the melt in Fe bearing minerals. Eventually, after the magma has crystallized out much of the Mg, Fe bearing minerals start to mineralize, enriching the sample in alkalis. Ultimately, this means this magma is following a more Fe rich liquid line of descent, analogous to a tholeiitic differentiation trend.

Some Tam McArthur Rim rocks have compositions that are derived from a dryer magma and this observation more closely follows data collected for the High Lava Plains than for the High Cascades (figure 12). More locally, we see the transition from wetter magmas to dryer magmas as silica content increases throughout the region. The Shevlin Park Tuff, Tumalo Tuff, and Todd Lake deposits all display a trend similar to Tam McArthur Rim (figure 13) (Kent, unpublished).

The general implication of more tholeiitic compositions is that the melting mechanism is dry, hot decompression. Within the geologic context of the Cascade Arc and Cascadia subduction, decompression melting is observed in the High Lava Plains of Oregon. The High Lava Plains are located in the back arc of the Cascades and are comprised of young volcanism that has moved across southeastern Oregon terminating at Newberry Volcano (Jordan et al., 2004). Decompression melting in southeastern Oregon is likely attributed to corner flow, or counterflow, of the mantle along the subducting slab (Till, 2017) (figure 20). Tam McArthur Rim rock compositions fall within the same compositional range as the High Lava Plains rocks (tholeiitic), it is possible that volcanism is partly attributed to this corner flow of the mantle
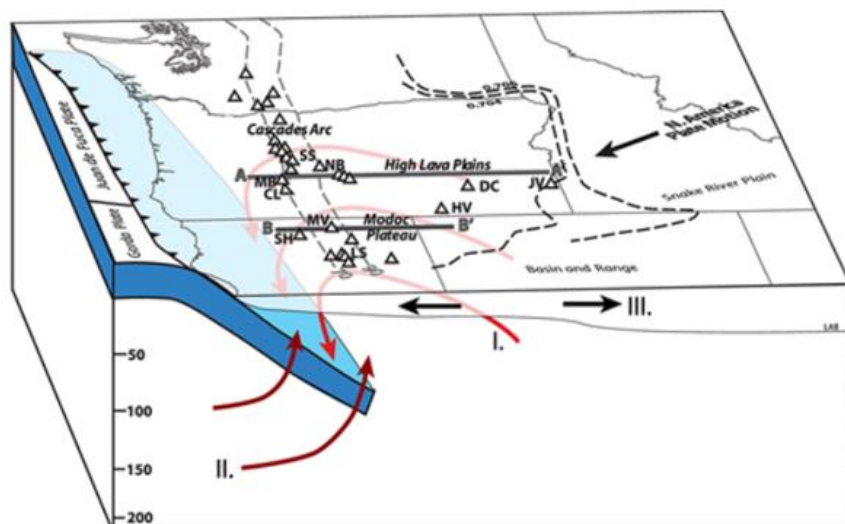


*Figure 20: Corner Flow along subducting slab (I) potentially causing anhydrous melts in southeastern Oregon and Northern California. Figure from (Till, 2017)*

(Till, 2017). Calc-alkaline rocks from Broken Top that overlie Tam McArthur Rim volcano are likely due to introduction of subducting slab fluids. However, because we also observe a few calc-alkaline rocks, it is likely two endmember styles of mantle melting are occurring. The two end members commonly observed together are decompression melting and fluid flux melting (Rowe et al., 2009).

## Mineral Chemistry

Petrographic analysis yielded an insightful look into microscopic scale textures of Tam McArthur Rim rocks. All samples have glomerocrystic clots of plagioclase, olivine, and pyroxene. I found that TMR-18-10, TMR-18-08, and TMR-18-04 are all crystal rich with felty textures meaning there is no flow fabric. All other samples have at least some trachytic fabric that presumably indicate flow direction. Many samples displayed a subophytic texture in the groundmass meaning plagioclase laths are larger than and enclose the pyroxenes. A subophytic texture implies a moderate cooling rate and represents the final melt in the system before eruption. Skeletal olivine replaced by subophytic groundmass was observed in TMR-18-04 and TMR-18-08 meaning the olivine is not in equilibrium with this system. These could either be xenocrysts or from an introduction of new magma into the system.

All samples have a plagioclase-dominant phenocryst phase. Plagioclase is observed as megacrysts, phenocrysts, and microlites. Some crystals exhibit significant disequilibrium sieve textures and oscillatory zoning while other crystals are euhedral. There is significant variation of plagioclase sizes and forms within individual thin sections. Plagioclase disequilibrium textures imply that the plagioclase was not in equilibrium at some point throughout its time in the magma. Some crystals show oscillatory zoning and multiple layers of sieve textures suggesting that they may have gone through multiple phases of both equilibrium and disequilibrium with the melt. To explore these plagioclase populations further, I used an electron microprobe to analyze individual plagioclase crystal compositions. Normal zoning means the system was evolving by crystallizing anorthite first and then albite, following normal cooling within the magma from more mafic to more felsic.

The goal of using the electron microprobe was to analyze the major elements of the three populations of plagioclase crystals observed. To have a general understanding of the crystals, I analyzed cores and rims of plagioclase crystals from TMR-16-01, TMR-18-04, TMR-18-08, and TMR-18-10. In general, cores had higher anorthite contents and rims had lower anorthite contents (figure 16). This means that cores are more calcic and rims are more sodic, this follows normal zoning. Both cores and rim had modes at $\sim An_{57}$.

The three plagioclase populations appear to vary by anorthite content (figure 17). Microlites had lower anorthite contents, with a mode of $\sim An_{50}$ but range from $\sim An_{37}$ to $\sim An_{75}$. Macrocrysts have higher anorthite contents in general having a mode around $\sim An_{60}$, but range from $\sim An_{37}$ to $\sim An_{87}$. Phenocrysts fall more in the middle of the An spectrum with a mode at $\sim An_{57}$ with two other minor modes at $\sim An_{48}$ and $\sim An_{67}$. This follows normal cooling within magma. Anorthite will crystallize first creating megacrysts leaving the melt relatively albite enriched. Phenocryst crystallization joins the megacrysts crystallization to drive the system to have an even more albite enriched melt. Finally, the groundmass microlites represent final stages of crystallization of the albite enriched melt.

Grouping anorthite content frequencies by silica content allows us to analyze anorthite by rock type (figure 18). This plot shows that the trachyte (TMR-16-01) has low anorthite contents with a mode at $\sim An_{37}$. Both TMR-18-10 and TMR-18-04 are basaltic andesites and have moderate anorthite contents with modes around $\sim An_{56}$ and $\sim An_{60}$ respectively. TMR-18-08 is a basaltic andesite and shows no significant mode of anorthite content. This follows what would be expected because trachytes are high in alkalis, driving it toward a more albite composition.

Several analyzed electron microprobe data points were disregarded because of their departures from an Si vs Al correlation. All of the samples, except TMR-16-01 show $R^2>0.98$ for a correlation of Si vs Al after data points are removed. TMR-16-01 ($R^2= 0.83$) did not have a higher $R^2$ value because data points were too sparse. I found that microlites ($\sim 30$ μm) were difficult to analyze because the resolution and refresh time on the microprobe display made it difficult to determine where these crystals

actually were. The beam diameter, 5μm, was too large and some crystal widths are on a similar order of magnitude making it especially difficult to analyze the microlites. In future studies, there needs to be a better approach to analyzing the microlites. Additionally, three of the samples analyzed (those from the TMR-18 suite), unintentionally are actually likely from Broken Top lavas that overlie Tam McArthur Rim lavas. Microprobe analysis of Tam McArthur Rim lavas from below the unconformity can shed more light on plagioclase compositions.

## Conclusions

Tam McArthur Rim is a small Central Oregon shield volcano in the High Cascades. According to our new $^{40}Ar/^{39}Ar$ ages, most of the lava flows that underlie the rhyodacite dome were extruded between 182.6 ka and 184.5 ka, likely within a ~10 kyr period. Our ages imply that the overlying dome's older K-Ar age of ~213 ka (Hill, 1991) may be incorrect based on the principle of superposition. Timing of the shift of eruptive focus that passed under Tam McArthur Rim is now better understood. Previous interpretations of when volcanism ceased in both the Tumalo Volcanic Fields and Broken Top systems at ~0.2 Ma can be adjusted to the younger age I acquired of < ~0.18 Ma.

Most samples from Tam McArthur Rim display tholeiitic compositions that are analogous to compositions of the High Lava Plains of Oregon, implying that the melt is anhydrous. Ultimately, the melt mechanism for these tholeiitic rocks is decompression melting. Because hydrous, calc-alkaline Broken Top lavas are found overlying Tam McArthur Rim lavas means Broken Top lava are from a hydrous magma. Melt generation that formed the Broken Top lavas and Tam McArthur Rim rocks in this study is likely from two processes: decompression melting and fluid flux melting.

Tam McArthur Rim is a unique location because it could represent a nexus of the High Lava Plains and High Cascades of Oregon. It is spatially located in the High Cascades, but is chemically analogous to the High Lava plains. Tam McArthur Rim may represent the most western extent of the High Lava Plains' decompression melting tholeiitic rocks.

# References

Hildreth, W. (2007). *Quaternary magmatism in the Cascades; geologic perspectives: U.S. Geological Survey professional Paper 1744 (125 pp).* USGS.

Hill, B. E., & Scott, W. E. (1990). Field trip guide to the central Oregon High Cascades Part 2 (conclusion): Ash-flow tuffs in the Bend area. Oregon Geology: DOGAMI, 52(6), 122-126.

Hill, B. E., (1992), *Petrogenesis of Compositionally Distinct Silicic Volcanoes in the Three Sister Region of the Oregon Cascade Range: The Effects of Crustal Extension on the Development of Continental Arc Silicic Magmatism.* Oregon State University [dissertation].

Jordan, B.T., Grunder, A.L., Duncan, R.A., Deino, A.L., 2004. Geochronology of age-progressive volcanism of the Oregon High Lava Plains: Implications for the plume interpretation of Yellowstone. Journal of Geophysical Research: Solid Earth 109, B10202. doi:10.1029/2003JB002776

Koppers, A.A.P., 2002. ArArCALC-software for 40Ar/39Ar age calculations. Computers & Geosciences 28 (5), 605–619.

Miyashiro, A., 1974. Volcanic rock series in island arcs and active continental margins. Am J Sci 274, 321–355. doi:10.2475/ajs.274.4.321

Pitcher, B.W., 2017,The Deschutes Formation: Evidence of Extension-Enhanced Explosivity in the Early High Cascades. Oregon State University [dissertation].

Rowe, M., Kent, A. J., & Nielsen, R. L. (2009, January 07). Subduction Influence on Oxygen Fugacity and Trace and Volatile Elements in Basalts Across the Cascade Volcanic Arc. Retrieved from https://doi.org/10.1093/petrology/egn072

Sherrod, D. R., Taylor, E. M., Ferns, M. L., Scott, W. E., Smith, G. A., & Conrey, R. M. (2004). *Geologic map of the Bend 30- x 60-Minute Quadrangle, Central Oregon.* USGS.

Sisson, T.W., Ratajeski, K., Hankins, W.B., Glazner, A.F., 2005. Voluminous granitic magmas from common basaltic sources. Contrib Mineral Petrol 148, 635–661. doi:10.1007/s00410-004-0632-9

Taylor, E. 1987. Field geology of the northwest quarter of the Broken Top 15 quadrangle, Deschutes County, Oregon: Special Paper 2. DOGAMI. doi:10.2172/6067987

Taylor, E.M., 1990. Volcanic history and tectonic development of the Central High Cascades Range, Oregon. Journal of Geophysical Research: Solid Earth 95, 19611–19622. doi:10.1029/JB095iB12p19611

Till, C.B., Grove, T.L., Carlson, R.W., Donnelly-Nolan, J.M., Fouch, M.J., Wagner, L.S., Hart, W.K., 2013. Depths and temperatures of <10.5 Ma mantle melting and the lithosphere-asthenosphere boundary below southern Oregon and northern California. Geochemistry, Geophysics, Geosystems 14, 864–879. doi:10.1002/ggge.20070

Till, C. (2017). A review and update of mantle thermobarometry for primitive arc magmas. American Mineralogist, 102(5), 931-947. doi.org/10.2138/am-2017-5783

# Appendix

Appendix A-1: Whole Rock major element geochemistry data from Washington State University XRF (16-) and Pomona College XRF(18-).

| Oxide | 16-01 | 16-02 | 16-03 | 18-03 | 18-04 | 18-05 | 18-06 | 18-07 | 18-08 | 18-10 |
|---|---|---|---|---|---|---|---|---|---|---|
| $SiO_2$ | 64.84 | 56.67 | 55.92 | 69.28 | 53.62 | 66.73 | 55.22 | 56.12 | 54.43 | 54.96 |
| $TiO_2$ | 0.93 | 1.53 | 1.27 | 0.56 | 0.99 | 0.69 | 1.49 | 1.29 | 0.95 | 0.87 |
| $Al_2O_3$ | 16.33 | 16.57 | 17.81 | 15.16 | 18.58 | 15.63 | 16.46 | 16.69 | 18.34 | 18.45 |
| FeO* | 5.47 | 9.18 | 8.25 | 3.69 | 7.75 | 4.93 | 10.05 | 9.19 | 7.60 | 7.66 |
| MnO | 0.12 | 0.15 | 0.14 | 0.11 | 0.18 | 0.14 | 0.16 | 0.15 | 0.12 | 0.12 |
| MgO | 1.12 | 3.12 | 3.43 | 0.53 | 5.61 | 0.79 | 3.47 | 3.47 | 5.24 | 5.08 |
| CaO | 3.21 | 6.82 | 7.72 | 1.76 | 8.41 | 2.38 | 7.22 | 6.92 | 8.25 | 7.96 |
| $Na_2O$ | 5.83 | 4.61 | 4.32 | 5.72 | 3.61 | 5.99 | 4.48 | 4.61 | 3.76 | 3.80 |
| $K_2O$ | 1.88 | 1.04 | 0.89 | 2.89 | 0.76 | 2.36 | 0.94 | 1.07 | 0.85 | 0.77 |
| $P2O_5$ | 0.28 | 0.31 | 0.25 | 0.11 | 0.24 | 0.18 | 0.31 | 0.29 | 0.24 | 0.13 |
| Total | 100.00 | 100.00 | 100.00 | 99.80 | 99.76 | 99.81 | 99.79 | 99.78 | 99.77 | 99.80 |

Appendix A-2: Whole rock trace element geochemistry: Washington State University ICP-MS.

| ppm | TMR-16-01 | TMR-16-02 | TMR-16-03 |
|---|---|---|---|
| La | 23.17 | 15.53 | 13.1 |
| Ce | 47.92 | 35.08 | 29.23 |
| Pr | 6.9 | 4.8 | 4.07 |
| Nd | 29.86 | 21.31 | 17.82 |
| Sm | 7.35 | 5.21 | 4.51 |
| Eu | 2.02 | 1.79 | 1.5 |
| Gd | 7.26 | 5.44 | 4.53 |
| Tb | 1.19 | 0.88 | 0.74 |
| Dy | 7.51 | 5.45 | 4.42 |
| Ho | 1.56 | 1.06 | 0.89 |
| Er | 4.25 | 2.85 | 2.4 |
| Tm | 0.6 | 0.4 | 0.34 |
| Yb | 3.86 | 2.55 | 2.14 |
| Lu | 0.6 | 0.39 | 0.33 |
| Ba | 573 | 402 | 350 |
| Th | 3.54 | 1.64 | 1.38 |
| Nb | 11.73 | 7.73 | 6.29 |
| Y | 39.9 | 27.03 | 22.62 |
| Hf | 6.09 | 3.66 | 3.12 |
| Ta | 0.77 | 0.48 | 0.39 |
| U | 1.42 | 0.71 | 0.58 |
| Pb | 8.19 | 10.15 | 4.4 |
| Rb | 34.6 | 16.6 | 13.6 |
| Cs | 0.84 | 0.25 | 0.31 |
| Sr | 322 | 512 | 564 |
| Sc | 15.2 | 27.9 | 25.1 |
| Zr | 242 | 146 | 123 |

Appendix A-3: Whole rock trace element geochemistry from Pomona College.

| Sample | TMR-18-03 | TMR-18-04 | TMR-18-05 | TMR-18-06 | TMR-18-07 | TMR-18-08 | TMR-18-10 |
|--------|-----------|-----------|-----------|-----------|-----------|-----------|-----------|
| Rb | 56.66 | 9.54 | 42.97 | 16.93 | 16.94 | 10.97 | 11.06 |
| Sr | 182.12 | 788.71 | 226.83 | 513.83 | 591.07 | 795.96 | 643.36 |
| Ba | 739.60 | 331.81 | 661.51 | 366.45 | 416.64 | 321.18 | 266.39 |
| Zr | 339.95 | 124.03 | 324.76 | 133.44 | 135.56 | 116.70 | 88.46 |
| Y | 38.45 | 19.08 | 47.96 | 24.89 | 22.93 | 16.96 | 15.08 |
| Nb | 18.21 | 9.54 | 19.99 | 9.96 | 8.97 | 7.98 | 5.03 |
| Cs | 0.00 | 0.00 | 0.00 | 0.00 | 0.00 | 0.00 | 0.00 |
| Sc | 7.08 | 20.14 | 7.99 | 27.88 | 25.92 | 22.94 | 24.13 |
| V | 15.18 | 166.44 | 18.99 | 278.82 | 224.27 | 144.63 | 159.83 |
| Cr | 5.06 | 115.55 | 0.00 | 15.93 | 15.95 | 80.79 | 88.46 |
| Ni | 10.12 | 109.19 | 0.00 | 4.98 | 6.98 | 93.76 | 84.44 |
| Cu | 22.26 | 65.73 | 5.00 | 107.55 | 70.77 | 57.85 | 59.31 |
| Zn | 70.82 | 136.75 | 84.94 | 93.60 | 90.70 | 71.82 | 67.35 |
| Ga | 19.22 | 19.08 | 19.99 | 18.92 | 19.93 | 19.95 | 19.10 |
| La | 25.29 | 11.66 | 35.97 | 18.92 | 22.93 | 15.96 | 11.06 |
| Ce | 63.74 | 29.68 | 59.96 | 33.86 | 37.88 | 28.93 | 30.16 |
| Pr | 6.07 | 3.18 | 7.99 | 3.98 | 5.98 | 3.99 | 3.02 |
| Nd | 24.28 | 11.66 | 31.98 | 19.92 | 21.93 | 13.96 | 18.09 |
| Hf | 7.08 | 0.00 | 6.00 | 1.99 | 3.99 | 1.99 | 3.02 |
| Pb | 9.11 | 0.00 | 8.99 | 1.99 | 1.99 | 0.00 | 0.00 |
| Th | 4.05 | 0.00 | 4.00 | 1.99 | 2.99 | 0.00 | 0.00 |
| U | 0.00 | 0.00 | 0.00 | 0.00 | 0.00 | 0.00 | 0.00 |

Appendix B-1: Oregon State University Electron Microprobe data: Weight %

| Point | Na | Si | Al | Fe | Ca | K | Mg | Ti | O | Total | X | Y | Z | Comment | Mean Z | Point# |
|---|---|---|---|---|---|---|---|---|---|---|---|---|---|---|---|---|
| 1/1. | 0.0349 | 25.5216 | 0.459 | 10.3976 | 1.4204 | 0 | 16.5096 | 0.1447 | 44.0099 | 98.4977 | 16997 | -5366 | 209 | TMR-18-08_Plag1 | 12.1578 | 1 |
| 1/2. | 0.1436 | 24.5425 | 0.8917 | 14.0198 | 1.6199 | 0.0075 | 13.9126 | 0.2438 | 42.7925 | 98.1738 | 16803 | -5519 | 206 | TMR-18-08_Plag1 | 12.6848 | 2 |
| 2/1. | 1.6995 | 22.2413 | 17.1742 | 0.3689 | 11.2476 | 0.0395 | 0.0547 | 0.0191 | 45.8614 | 98.7062 | 19133 | -10495 | 180 | TMR-18-08_Plag2 | 11.566 | 3 |
| 2/2. | 1.2737 | 21.8041 | 17.6193 | 0.3969 | 11.8316 | 0.0487 | 0.0458 | 0.0197 | 45.8486 | 98.8883 | 18572 | -10481 | 175 | TMR-18-08_Plag2 | 11.6397 | 4 |
| 2/3. | 1.8723 | 22.9471 | 16.8374 | 0.4991 | 10.6284 | 0.0862 | 0.036 | 0.0187 | 46.2133 | 99.1386 | 18067 | -10608 | 176 | TMR-18-08_Plag2 | 11.5847 | 5 |
| 3/1. | 1.35 | 22.0932 | 17.5605 | 0.466 | 11.6993 | 0.0583 | 0.0325 | 0.0045 | 46.1023 | 99.3665 | 20206 | -15319 | 149 | TMR-18-08_Plag3 | 11.6896 | 6 |
| 3/2. | 1.7581 | 22.8131 | 17.0721 | 0.3899 | 10.9687 | 0.0672 | 0.0642 | 0.0265 | 46.354 | 99.5137 | 19896 | -15359 | 146 | TMR-18-08_Plag3 | 11.6363 | 7 |
| 3/3. | 3.088 | 24.5426 | 15.3826 | 0.6044 | 8.5279 | 0.193 | 0.0449 | 0.0414 | 46.3948 | 98.8196 | 19570 | -15384 | 146 | TMR-18-08_Plag3 | 11.4009 | 8 |
| 4/1. | 2.6558 | 24.1489 | 15.59 | 0.7472 | 9.2153 | 0.1886 | 0.053 | 0.0426 | 46.3007 | 98.9421 | 12366 | -25656 | 57 | TMR-18-08_Plag4 | 11.4926 | 9 |
| 4/2. | 4.0285 | 26.1996 | 14.1906 | 0.7146 | 6.808 | 0.3592 | 0.0536 | 0.0679 | 46.9521 | 99.3741 | 12518 | -25806 | 57 | TMR-18-08_Plag4 | 11.3491 | 10 |
| 5/1. | 3.4214 | 24.9779 | 14.9822 | 0.5616 | 7.8719 | 0.1964 | 0.0764 | 0.0378 | 46.3954 | 98.521 | 12989 | -25687 | 59 | TMR-18-08_Plag5 | 11.3078 | 11 |
| 5/2. | 2.9112 | 24.1428 | 15.7518 | 0.6049 | 9.1256 | 0.1797 | 0.0595 | 0.0425 | 46.4525 | 99.2706 | 13001 | -25699 | 59 | TMR-18-08_Plag5 | 11.4972 | 12 |
| 5/3. | 4.1562 | 26.5808 | 13.9876 | 0.6898 | 6.4678 | 0.4134 | 0.042 | 0.065 | 47.1089 | 99.5115 | 13009 | -25704 | 57 | TMR-18-08_Plag5 | 11.3364 | 13 |
| 6/1. | 2.5071 | 23.0316 | 15.5866 | 0.6666 | 9.2547 | 0.1825 | 0.0348 | 0.0434 | 44.9529 | 96.2603 | 6471 | -38900 | -48 | TMR-18-08_Plag6 | 11.1954 | 14 |
| 6/2. | 3.8736 | 25.693 | 14.1992 | 0.8272 | 6.7864 | 0.3413 | 0.0432 | 0.071 | 46.3437 | 98.1785 | 6472 | -38908 | -45 | TMR-18-08_Plag6 | 11.2345 | 15 |
| 7/1. | 1.2882 | 21.8395 | 17.631 | 0.3855 | 12.07 | 0.0434 | 0.0588 | 0.0147 | 46.0004 | 99.3314 | -23495 | -8050 | 80 | TMR-18-04_Plag1 | 11.7041 | 16 |
| 7/2. | 3.0896 | 24.7741 | 15.4269 | 0.5196 | 8.6389 | 0.1614 | 0.0873 | 0.0373 | 46.7371 | 99.4721 | -23345 | -8188 | 79 | TMR-18-04_Plag1 | 11.4649 | 17 |
| 8/1. | 1.4197 | 22.0397 | 17.4088 | 0.4095 | 11.5594 | 0.0693 | 0.0453 | 0.0116 | 45.8742 | 98.8378 | -8605 | -5855 | 142 | TMR-18-04_Plag2 | 11.6144 | 18 |
| 8/2. | 3.2385 | 24.7029 | 15.2011 | 0.4855 | 8.3506 | 0.1494 | 0.1037 | 0.0346 | 46.3886 | 98.6549 | -8802 | -5655 | 148 | TMR-18-04_Plag2 | 11.3467 | 19 |
| 8/3. | 2.7162 | 24.4694 | 14.9592 | 1.3011 | 8.7616 | 0.2377 | 0.4585 | 0.1221 | 46.4336 | 99.4595 | -8766 | -5502 | 148 | TMR-18-04_Plag2 | 11.6015 | 20 |
| 8/4. | 2.6958 | 23.9441 | 15.83 | 0.4516 | 9.4225 | 0.1066 | 0.0851 | 0.0256 | 46.2858 | 98.8471 | -8795 | -5465 | 146 | TMR-18-04_Plag2 | 11.4475 | 21 |
| 9/1. | 3.5076 | 26.0011 | 14.6772 | 0.4609 | 7.4479 | 0.1921 | 0.092 | 0.0439 | 47.1352 | 99.5578 | -15542 | -36024 | -102 | TMR-18-04_Plag3 | 11.3714 | 22 |
| 9/2. | 2.4777 | 23.9942 | 16.1717 | 0.4343 | 9.7018 | 0.1033 | 0.0786 | 0.0317 | 46.6766 | 99.6698 | -15748 | -35988 | -101 | TMR-18-04_Plag3 | 11.5575 | 23 |
| 9/3. | 3.108 | 24.7205 | 15.5456 | 0.545 | 8.5957 | 0.1561 | 0.0971 | 0.0379 | 46.7838 | 99.5895 | -15799 | -35943 | -98 | TMR-18-04_Plag3 | 11.4769 | 24 |
| 10/1. | 2.5261 | 23.9795 | 16.0554 | 0.5222 | 9.524 | 0.106 | 0.0841 | 0.0301 | 46.5306 | 99.358 | -16051 | -35888 | -101 | TMR-18-04_Plag4 | 11.5221 | 25 |
| 10/2. | 3.2198 | 24.9885 | 15.2175 | 0.5557 | 8.3433 | 0.1433 | 0.0943 | 0.0479 | 46.7407 | 99.3509 | -16078 | -35902 | -99 | TMR-18-04_Plag4 | 11.4323 | 26 |
| 10/3. | 3.4053 | 25.409 | 14.9343 | 0.594 | 8.0673 | 0.2003 | 0.1006 | 0.0494 | 46.9502 | 99.7105 | -16094 | -35912 | -100 | TMR-18-04_Plag4 | 11.4582 | 27 |
| 11/1. | 3.5338 | 25.0418 | 14.771 | 0.6572 | 7.675 | 0.2187 | 0.0952 | 0.064 | 46.3028 | 98.3596 | -4858 | -39813 | -90 | TMR-18-04_Plag5 | 11.292 | 28 |
| 11/2. | 4.3222 | 27.2541 | 12.9417 | 0.9851 | 5.6206 | 0.5623 | 0.0732 | 0.1598 | 46.8641 | 98.783 | -4889 | -39804 | -94 | TMR-18-04_Plag5 | 11.2536 | 29 |
| 12/1. | 4.2554 | 26.5836 | 13.7004 | 0.7502 | 6.3027 | 0.3538 | 0.0662 | 0.0858 | 46.8602 | 98.9583 | -8513 | -40020 | -107 | TMR-18-04_Plag6 | 11.2693 | 30 |
| 12/2. | 3.5324 | 29.2985 | 7.7761 | 4.3026 | 2.4482 | 1.8938 | 0.3011 | 0.993 | 44.9871 | 95.5329 | -8518 | -40020 | -111 | TMR-18-04_Plag6 | 11.323 | 31 |
| 13/1. | 3.2824 | 24.8687 | 15.2692 | 0.535 | 8.3523 | 0.1661 | 0.0802 | 0.0335 | 46.6555 | 99.243 | 6847 | 37836 | 408 | TMR-18-10_Plag1 | 11.4183 | 32 |
| 13/2. | 3.2538 | 24.551 | 15.199 | 0.5875 | 8.3549 | 0.1931 | 0.0841 | 0.0442 | 46.2525 | 98.5201 | 7177 | 37740 | 412 | TMR-18-10_Plag1 | 11.3514 | 33 |
| 13/3. | 2.2014 | 23.4539 | 16.7217 | 0.5489 | 10.4295 | 0.1327 | 0.0834 | 0.0297 | 46.7852 | 100.386 | 7232 | 37782 | 409 | TMR-18-10_Plag1 | 11.7127 | 34 |
| 13/4. | 3.7741 | 27.5469 | 12.0305 | 1.8382 | 5.3364 | 0.8561 | 0.0959 | 0.452 | 46.5978 | 98.5279 | 7246 | 37796 | 410 | TMR-18-10_Plag1 | 11.3823 | 35 |
| 14/1. | 3.7373 | 25.5768 | 14.7622 | 0.7101 | 7.5128 | 0.2523 | 0.0531 | 0.0612 | 46.9029 | 99.5686 | 7485 | 37854 | 411 | TMR-18-10_Plag2 | 11.4181 | 36 |
| 14/2. | 3.6927 | 25.5643 | 14.8752 | 0.6439 | 7.5823 | 0.2182 | 0.0644 | 0.0441 | 46.9714 | 99.6563 | 7477 | 37847 | 410 | TMR-18-10_Plag2 | 11.4194 | 37 |
| 15/1. | 4.0067 | 25.1874 | 14.6017 | 0.5101 | 7.6891 | 0.2248 | 0.0796 | 0.0509 | 46.4283 | 98.7787 | 20666 | 40016 | 439 | TMR-18-10_Plag3 | 11.3134 | 38 |
| 15/2. | 3.1878 | 24.6697 | 15.4884 | 0.5353 | 8.5624 | 0.1464 | 0.0808 | 0.0351 | 46.6721 | 99.3778 | 20513 | 39956 | 441 | TMR-18-10_Plag3 | 11.4486 | 39 |
| 15/3. | 3.3818 | 25.0575 | 15.0332 | 0.546 | 8.2127 | 0.1551 | 0.0805 | 0.0457 | 46.6489 | 99.1615 | 20388 | 39931 | 441 | TMR-18-10_Plag3 | 11.4 | 40 |
| 16/1. | 3.8787 | 29.0153 | 12.0379 | 0.8211 | 5.1956 | 0.4348 | 0.0532 | 0.1424 | 47.6451 | 99.2241 | 18131 | 41055 | 439 | TMR-18-10_Plag4 | 11.2383 | 41 |
| 16/2. | 3.6782 | 25.4616 | 14.8083 | 0.727 | 7.7084 | 0.2345 | 0.0448 | 0.0451 | 46.8552 | 99.5631 | 18131 | 41051 | 441 | TMR-18-10_Plag4 | 11.4333 | 42 |
| 17/1. | 3.4019 | 25.3062 | 15.0538 | 0.5345 | 8.2462 | 0.1769 | 0.0787 | 0.0422 | 46.9684 | 99.8086 | 10896 | 34471 | 397 | TMR-18-10_Plag5 | 11.4721 | 43 |
| 17/2. | 3.3679 | 25.1022 | 15.2196 | 0.5079 | 8.1967 | 0.1918 | 0.0824 | 0.0301 | 46.8417 | 99.5403 | 10828 | 34595 | 399 | TMR-18-10_Plag5 | 11.435 | 44 |
| 17/3. | 3.4019 | 25.2648 | 15.0331 | 0.528 | 8.1138 | 0.1746 | 0.0833 | 0.0469 | 46.8539 | 99.5003 | 10794 | 34635 | 399 | TMR-18-10_Plag5 | 11.4274 | 45 |
| 18/1. | 5.1882 | 28.093 | 13.2866 | 0.2449 | 4.7671 | 0.4633 | 0.0094 | 0.0176 | 47.7181 | 99.7882 | -8174 | 20412 | 308 | TMR-16-01_Plag1 | 11.5186 | 46 |
| 18/2. | 4.3989 | 26.8402 | 14.2289 | 0.3717 | 6.2304 | 0.2971 | 0.0154 | 0.0292 | 47.4523 | 99.8641 | -8122 | 20295 | 311 | TMR-16-01_Plag1 | 11.2949 | 47 |
| 19/1. | 4.7939 | 27.0356 | 13.6294 | 0.2741 | 5.5692 | 0.306 | 0.0115 | 0.0305 | 46.9874 | 98.6375 | -11491 | 14519 | 263 | TMR-16-01_Plag2 | 11.0945 | 48 |
| 19/2. | 4.2095 | 26.3528 | 14.3031 | 0.3717 | 6.5952 | 0.2174 | 0.0242 | 0.0316 | 47.0339 | 99.1395 | -11592 | 14519 | 259 | TMR-16-01_Plag2 | 11.2414 | 49 |
| 20/1. | 4.2704 | 28.919 | 8.3202 | 6.0836 | 1.8954 | 1.0827 | 0.4822 | 1.0658 | 45.5868 | 97.706 | -11885 | 13660 | 254 | TMR-16-01_Plag3 | 11.7058 | 50 |
| 20/2. | 5.0011 | 28.3 | 13.147 | 0.5886 | 4.7997 | 0.5287 | 0.0258 | 0.0525 | 47.9236 | 100.367 | -11868 | 13695 | 254 | TMR-16-01_Plag3 | 11.2832 | 51 |
| 21/1. | 4.0755 | 26.5695 | 10.7234 | 3.2439 | 5.6186 | 0.6015 | 1.0864 | 0.1662 | 45.3508 | 97.4358 | -12197 | 14176 | 258 | TMR-16-01_Plag4 | 11.4385 | 52 |
| 21/2. | 4.7701 | 27.4676 | 13.3709 | 0.6064 | 5.0059 | 0.7169 | 0.0173 | 0.0506 | 47.213 | 99.2186 | -12213 | 14155 | 259 | TMR-16-01_Plag4 | 11.1937 | 53 |

Appendix B-2: Oregon State University Electron Microprobe data: Atomic %

| Point | Na | Si | Al | Fe | Ca | K | Mg | Ti | O | Total | X | Y | Z | Comment | Mean Z | Point# |
|---|---|---|---|---|---|---|---|---|---|---|---|---|---|---|---|---|
| 1 / 1. | 0.0331 | 19.8332 | 0.3713 | 4.0635 | 0.7735 | 0 | 14.8254 | 0.0659 | 60.0341 | 100 | 16997 | -5366 | 209 | TMR-18-08_Plag1 | 12.1578 | 1 |
| 1 / 2. | 0.1401 | 19.6069 | 0.7415 | 5.6327 | 0.9069 | 0.0043 | 12.8436 | 0.1142 | 60.0098 | 100 | 16803 | -5519 | 206 | TMR-18-08_Plag1 | 12.6848 | 2 |
| 2 / 1. | 1.5865 | 16.9954 | 13.6603 | 0.1418 | 6.0226 | 0.0217 | 0.0483 | 0.0086 | 61.515 | 100 | 19133 | -10495 | 180 | TMR-18-08_Plag2 | 11.566 | 3 |
| 2 / 2. | 1.1898 | 16.6736 | 14.0247 | 0.1526 | 6.34 | 0.0268 | 0.0405 | 0.0088 | 61.5432 | 100 | 18572 | -10481 | 175 | TMR-18-08_Plag2 | 11.6397 | 4 |
| 2 / 3. | 1.7369 | 17.4245 | 13.3083 | 0.1906 | 5.6553 | 0.047 | 0.0316 | 0.0083 | 61.5975 | 100 | 18067 | -10608 | 176 | TMR-18-08_Plag2 | 11.5847 | 5 |
| 3 / 1. | 1.2545 | 16.8059 | 13.9044 | 0.1783 | 6.2361 | 0.0319 | 0.0285 | 0.002 | 61.5584 | 100 | 20206 | -15319 | 149 | TMR-18-08_Plag3 | 11.6896 | 6 |
| 3 / 2. | 1.6256 | 17.267 | 13.4504 | 0.1484 | 5.8176 | 0.0366 | 0.0562 | 0.0118 | 61.5865 | 100 | 19896 | -15359 | 146 | TMR-18-08_Plag3 | 11.6363 | 7 |
| 3 / 3. | 2.8523 | 18.5562 | 12.1064 | 0.2298 | 4.5182 | 0.1048 | 0.0393 | 0.0184 | 61.5746 | 100 | 19570 | -15384 | 146 | TMR-18-08_Plag3 | 11.4009 | 8 |
| 4 / 1. | 2.4589 | 18.3015 | 12.2985 | 0.2848 | 4.8939 | 0.1027 | 0.0464 | 0.0189 | 61.5945 | 100 | 12366 | -25656 | 57 | TMR-18-08_Plag4 | 11.4926 | 9 |
| 4 / 2. | 3.6782 | 19.5812 | 11.0399 | 0.2686 | 3.5655 | 0.1929 | 0.0463 | 0.0298 | 61.5977 | 100 | 12518 | -25806 | 57 | TMR-18-08_Plag4 | 11.3491 | 10 |
| 5 / 1. | 3.1607 | 18.8879 | 11.7929 | 0.2136 | 4.1712 | 0.1067 | 0.0667 | 0.0168 | 61.5837 | 100 | 12989 | -25687 | 59 | TMR-18-08_Plag5 | 11.3078 | 11 |
| 5 / 2. | 2.683 | 18.2131 | 12.3692 | 0.2295 | 4.8241 | 0.0974 | 0.0519 | 0.0188 | 61.5131 | 100 | 13001 | -25699 | 59 | TMR-18-08_Plag5 | 11.4972 | 12 |
| 5 / 3. | 3.7843 | 19.8108 | 10.8516 | 0.2585 | 3.3779 | 0.2213 | 0.0362 | 0.0284 | 61.6311 | 100 | 13009 | -25704 | 57 | TMR-18-08_Plag5 | 11.3364 | 13 |
| 6 / 1. | 2.3882 | 17.9592 | 12.6511 | 0.2614 | 5.0569 | 0.1022 | 0.0314 | 0.0199 | 61.5297 | 100 | 6471 | -38900 | -48 | TMR-18-08_Plag6 | 11.1954 | 14 |
| 6 / 2. | 3.5833 | 19.4551 | 11.1918 | 0.315 | 3.6009 | 0.1856 | 0.0378 | 0.0315 | 61.599 | 100 | 6472 | -38908 | -45 | TMR-18-08_Plag6 | 11.2345 | 15 |
| 7 / 1. | 1.1988 | 16.6368 | 13.9805 | 0.1477 | 6.443 | 0.0238 | 0.0517 | 0.0066 | 61.5112 | 100 | -23495 | -8050 | 80 | TMR-18-04_Plag1 | 11.7041 | 16 |
| 7 / 2. | 2.8336 | 18.5992 | 12.0556 | 0.1962 | 4.5447 | 0.087 | 0.0757 | 0.0164 | 61.5915 | 100 | -23345 | -8188 | 79 | TMR-18-04_Plag1 | 11.4649 | 17 |
| 8 / 1. | 1.3257 | 16.8454 | 13.8503 | 0.1574 | 6.1911 | 0.0381 | 0.04 | 0.0052 | 61.5469 | 100 | -8605 | -5855 | 142 | TMR-18-04_Plag2 | 11.6144 | 18 |
| 8 / 2. | 2.9915 | 18.6784 | 11.9642 | 0.1846 | 4.4245 | 0.0811 | 0.0906 | 0.0153 | 61.5698 | 100 | -8802 | -5655 | 148 | TMR-18-04_Plag2 | 11.3467 | 19 |
| 8 / 3. | 2.5057 | 18.4769 | 11.7579 | 0.4941 | 4.636 | 0.1289 | 0.4001 | 0.0541 | 61.5463 | 100 | -8766 | -5502 | 148 | TMR-18-04_Plag2 | 11.6015 | 20 |
| 8 / 4. | 2.4953 | 18.1419 | 12.4848 | 0.1721 | 5.0027 | 0.058 | 0.0745 | 0.0114 | 61.5595 | 100 | -8795 | -5465 | 146 | TMR-18-04_Plag2 | 11.4475 | 21 |
| 9 / 1. | 3.1972 | 19.4004 | 11.3993 | 0.173 | 3.8941 | 0.103 | 0.0793 | 0.0192 | 61.7346 | 100 | -15542 | -36024 | -102 | TMR-18-04_Plag3 | 11.3714 | 22 |
| 9 / 2. | 2.276 | 18.0423 | 12.6577 | 0.1642 | 5.112 | 0.0558 | 0.0683 | 0.014 | 61.6096 | 100 | -15748 | -35988 | -101 | TMR-18-04_Plag3 | 11.5575 | 23 |
| 9 / 3. | 2.847 | 18.536 | 12.1334 | 0.2055 | 4.5164 | 0.0841 | 0.0841 | 0.0167 | 61.5769 | 100 | -15799 | -35943 | -98 | TMR-18-04_Plag3 | 11.4769 | 24 |
| 10 / 1. | 2.3276 | 18.0865 | 12.6052 | 0.1981 | 5.0337 | 0.0574 | 0.0733 | 0.0133 | 61.6049 | 100 | -16051 | -35888 | -101 | TMR-18-04_Plag4 | 11.5221 | 25 |
| 10 / 2. | 2.9536 | 18.7638 | 11.8943 | 0.2098 | 4.3901 | 0.0773 | 0.0818 | 0.0211 | 61.6083 | 100 | -16078 | -35902 | -99 | TMR-18-04_Plag4 | 11.4323 | 26 |
| 10 / 3. | 3.1099 | 18.9946 | 11.621 | 0.2233 | 4.226 | 0.1076 | 0.0869 | 0.0216 | 61.609 | 100 | -16094 | -35912 | -100 | TMR-18-04_Plag4 | 11.4582 | 27 |
| 11 / 1. | 3.2699 | 18.9674 | 11.6458 | 0.2503 | 4.0736 | 0.119 | 0.0833 | 0.0284 | 61.5622 | 100 | -4858 | -39813 | -90 | TMR-18-04_Plag5 | 11.292 | 28 |
| 11 / 2. | 3.9616 | 20.4481 | 10.1071 | 0.3717 | 2.955 | 0.3031 | 0.0634 | 0.0703 | 61.7198 | 100 | -4889 | -39804 | -94 | TMR-18-04_Plag5 | 11.2536 | 29 |
| 12 / 1. | 3.8949 | 19.9167 | 10.6844 | 0.2827 | 3.3089 | 0.1904 | 0.0573 | 0.0377 | 61.627 | 100 | -8513 | -40020 | -107 | TMR-18-04_Plag6 | 11.2693 | 30 |
| 12 / 2. | 3.402 | 23.0977 | 6.3812 | 1.7058 | 1.3524 | 1.0725 | 0.2743 | 0.459 | 62.255 | 100 | -8518 | -40020 | -111 | TMR-18-04_Plag6 | 11.323 | 31 |
| 13 / 1. | 3.0145 | 18.6951 | 11.9483 | 0.2023 | 4.3998 | 0.0897 | 0.0696 | 0.0148 | 61.566 | 100 | 6847 | 37836 | 408 | TMR-18-10_Plag1 | 11.4183 | 32 |
| 13 / 2. | 3.0126 | 18.6065 | 11.9903 | 0.2239 | 4.437 | 0.1051 | 0.0737 | 0.0197 | 61.5312 | 100 | 7177 | 37740 | 412 | TMR-18-10_Plag1 | 11.3514 | 33 |
| 13 / 3. | 2.015 | 17.5728 | 13.0413 | 0.2068 | 5.4758 | 0.0714 | 0.0722 | 0.013 | 61.5317 | 100 | 7232 | 37782 | 409 | TMR-18-10_Plag1 | 11.7127 | 34 |
| 13 / 4. | 3.4894 | 20.8483 | 9.4776 | 0.6996 | 2.8301 | 0.4654 | 0.0839 | 0.2006 | 61.9051 | 100 | 7246 | 37796 | 410 | TMR-18-10_Plag1 | 11.3823 | 35 |
| 14 / 1. | 3.4139 | 19.1243 | 11.4896 | 0.267 | 3.9364 | 0.1355 | 0.0459 | 0.0268 | 61.5606 | 100 | 7485 | 37854 | 411 | TMR-18-10_Plag2 | 11.4181 | 36 |
| 14 / 2. | 3.3689 | 19.0915 | 11.5633 | 0.2418 | 3.9679 | 0.1171 | 0.0555 | 0.0193 | 61.5747 | 100 | 7477 | 37847 | 410 | TMR-18-10_Plag3 | 11.4194 | 37 |
| 15 / 1. | 3.6884 | 18.9797 | 11.4532 | 0.1933 | 4.0601 | 0.1217 | 0.0693 | 0.0225 | 61.4119 | 100 | 20666 | 40016 | 439 | TMR-18-10_Plag3 | 11.3134 | 38 |
| 15 / 2. | 2.9259 | 18.5347 | 12.1127 | 0.2023 | 4.5078 | 0.079 | 0.0701 | 0.0155 | 61.552 | 100 | 20513 | 39956 | 441 | TMR-18-10_Plag3 | 11.4486 | 39 |
| 15 / 3. | 3.1067 | 18.8426 | 11.7672 | 0.2065 | 4.3276 | 0.0838 | 0.0699 | 0.0202 | 61.5756 | 100 | 20388 | 39931 | 441 | TMR-18-10_Plag3 | 11.4 | 40 |
| 16 / 1. | 3.5249 | 21.5841 | 9.3212 | 0.3072 | 2.7083 | 0.2324 | 0.0457 | 0.0621 | 62.2141 | 100 | 18131 | 41055 | 439 | TMR-18-10_Plag4 | 11.2383 | 41 |
| 16 / 2. | 3.3626 | 19.0538 | 11.5349 | 0.2736 | 4.0422 | 0.1261 | 0.0387 | 0.0198 | 61.5484 | 100 | 18131 | 41051 | 441 | TMR-18-10_Plag4 | 11.4333 | 42 |
| 17 / 1. | 3.1045 | 18.9039 | 11.7054 | 0.2008 | 4.3165 | 0.0949 | 0.068 | 0.0185 | 61.5876 | 100 | 10896 | 34471 | 397 | TMR-18-10_Plag5 | 11.4721 | 43 |
| 17 / 2. | 3.0812 | 18.7986 | 11.8641 | 0.1913 | 4.3014 | 0.1032 | 0.0713 | 0.0132 | 61.5758 | 100 | 10828 | 34595 | 399 | TMR-18-10_Plag5 | 11.435 | 44 |
| 17 / 3. | 3.1127 | 18.9229 | 11.7203 | 0.1989 | 4.2584 | 0.0939 | 0.0721 | 0.0206 | 61.6001 | 100 | 10794 | 34635 | 399 | TMR-18-10_Plag5 | 11.4274 | 45 |
| 18 / 1. | 4.6659 | 20.6808 | 10.1812 | 0.0907 | 2.4591 | 0.245 | 0.008 | 0.0076 | 61.6618 | 100 | -8174 | 20412 | 308 | TMR-16-01_Plag1 | 11.1586 | 46 |
| 18 / 2. | 3.9771 | 19.8637 | 10.9613 | 0.1383 | 3.2311 | 0.158 | 0.0132 | 0.0127 | 61.6447 | 100 | -8122 | 20295 | 311 | TMR-16-01_Plag1 | 11.2949 | 47 |
| 19 / 1. | 4.3754 | 20.1985 | 10.5993 | 0.103 | 2.9156 | 0.1642 | 0.0099 | 0.0133 | 61.6208 | 100 | -11491 | 14519 | 263 | TMR-16-01_Plag2 | 11.0945 | 48 |
| 19 / 2. | 3.839 | 19.6728 | 11.1144 | 0.1395 | 3.45 | 0.1166 | 0.0209 | 0.0138 | 61.633 | 100 | -11592 | 14519 | 259 | TMR-16-01_Plag2 | 11.2414 | 49 |
| 20 / 1. | 4.0389 | 22.3892 | 6.7051 | 2.3686 | 1.0283 | 0.6021 | 0.4314 | 0.4838 | 61.9525 | 100 | -11885 | 13660 | 254 | TMR-16-01_Plag3 | 11.7058 | 50 |
| 20 / 2. | 4.4819 | 20.7605 | 10.039 | 0.2171 | 2.4673 | 0.2786 | 0.0219 | 0.0226 | 61.7111 | 100 | -11868 | 13695 | 254 | TMR-16-01_Plag5 | 11.2832 | 51 |
| 21 / 1. | 3.8396 | 20.49 | 8.6081 | 1.2581 | 3.0363 | 0.3332 | 0.9681 | 0.0751 | 61.3914 | 100 | -12197 | 14176 | 258 | TMR-16-01_Plag4 | 11.4385 | 52 |
| 21 / 2. | 4.3337 | 20.4272 | 10.3506 | 0.2268 | 2.6087 | 0.383 | 0.0149 | 0.0221 | 61.6331 | 100 | -12213 | 14155 | 259 | TMR-16-01_Plag4 | 11.1937 | 53 |

Appendix B-3: Oregon State University Electron Microprobe data: Oxide %

| Point | Na2O | SiO2 | Al2O3 | FeO | CaO | K2O | MgO | TiO2 | Total | X | Y | Z | Commen | Mean Z | Point# |
|---|---|---|---|---|---|---|---|---|---|---|---|---|---|---|---|
| 1 / 1. | 0.0471 | 54.6003 | 0.8673 | 13.3765 | 1.9874 | 0 | 27.3778 | 0.2414 | 98.4977 | 16997 | -5366 | 209 | R-18-08_F | 12.1578 | 1 |
| 1 / 2. | 0.1936 | 52.5056 | 1.6848 | 18.0364 | 2.2666 | 0.009 | 23.0713 | 0.4066 | 98.1738 | 16803 | -5519 | 206 | R-18-08_F | 12.6848 | 2 |
| 2 / 1. | 2.2909 | 47.5825 | 32.4504 | 0.4746 | 15.7376 | 0.0476 | 0.0906 | 0.0319 | 98.7062 | 19133 | -10495 | 180 | R-18-08_F | 11.566 | 3 |
| 2 / 2. | 1.7169 | 46.6471 | 33.2915 | 0.5106 | 16.5548 | 0.0587 | 0.0759 | 0.0329 | 98.8883 | 18572 | -10481 | 175 | R-18-08_F | 11.6397 | 4 |
| 2 / 3. | 2.5239 | 49.0924 | 31.8141 | 0.6421 | 14.8712 | 0.1039 | 0.0597 | 0.0312 | 99.1386 | 18067 | -10608 | 176 | R-18-08_F | 11.5847 | 5 |
| 3 / 1. | 1.8197 | 47.2656 | 33.1804 | 0.5995 | 16.3696 | 0.0702 | 0.0539 | 0.0075 | 99.3665 | 20206 | -15319 | 149 | R-18-08_F | 11.6896 | 6 |
| 3 / 2. | 2.3698 | 48.8056 | 32.2576 | 0.5016 | 15.3474 | 0.081 | 0.1065 | 0.0442 | 99.5137 | 19896 | -15359 | 146 | R-18-08_F | 11.6363 | 7 |
| 3 / 3. | 4.1625 | 52.5058 | 29.0654 | 0.7776 | 11.9322 | 0.2324 | 0.0745 | 0.0691 | 98.8196 | 19570 | -15384 | 146 | R-18-08_F | 11.4009 | 8 |
| 4 / 1. | 3.58 | 51.6634 | 29.4571 | 0.9613 | 12.894 | 0.2272 | 0.0879 | 0.0711 | 98.9421 | 12366 | -25656 | 57 | R-18-08_F | 11.4926 | 9 |
| 4 / 2. | 5.4303 | 56.0507 | 26.8131 | 0.9193 | 9.5257 | 0.4328 | 0.0889 | 0.1133 | 99.3741 | 12518 | -25806 | 57 | R-18-08_F | 11.3491 | 10 |
| 5 / 1. | 4.612 | 53.437 | 28.3089 | 0.7225 | 11.0144 | 0.2365 | 0.1267 | 0.0631 | 98.521 | 12989 | -25687 | 59 | R-18-08_F | 11.3078 | 11 |
| 5 / 2. | 3.9243 | 51.6505 | 29.763 | 0.7782 | 12.7686 | 0.2165 | 0.0986 | 0.0708 | 99.2706 | 13001 | -25699 | 59 | R-18-08_F | 11.4972 | 12 |
| 5 / 3. | 5.6025 | 56.8662 | 26.4295 | 0.8874 | 9.0497 | 0.498 | 0.0697 | 0.1084 | 99.5115 | 13009 | -25704 | 57 | R-18-08_F | 11.3364 | 13 |
| 6 / 1. | 3.3795 | 49.2733 | 29.4507 | 0.8576 | 12.9492 | 0.2198 | 0.0578 | 0.0725 | 96.2603 | 6471 | -38900 | -48 | R-18-08_F | 11.1954 | 14 |
| 6 / 2. | 5.2215 | 54.9669 | 26.8293 | 1.0642 | 9.4955 | 0.4111 | 0.0716 | 0.1184 | 98.1785 | 6472 | -38908 | -45 | R-18-08_F | 11.2345 | 15 |
| 7 / 1. | 1.7364 | 46.7228 | 33.3137 | 0.4959 | 16.8883 | 0.0523 | 0.0975 | 0.0245 | 99.3314 | -23495 | -8050 | 80 | R-18-04_F | 11.7041 | 16 |
| 7 / 2. | 4.1647 | 53.001 | 29.1491 | 0.6684 | 12.0876 | 0.1944 | 0.1447 | 0.0623 | 99.4721 | -23345 | -8188 | 79 | R-18-04_F | 11.4649 | 17 |
| 8 / 1. | 1.9138 | 47.1512 | 32.8939 | 0.5269 | 16.174 | 0.0835 | 0.0751 | 0.0194 | 98.8377 | -8605 | -5855 | 142 | R-18-04_F | 11.6144 | 18 |
| 8 / 2. | 4.3654 | 52.8487 | 28.7224 | 0.6246 | 11.6842 | 0.1799 | 0.172 | 0.0577 | 98.6549 | -8802 | -5655 | 148 | R-18-04_F | 11.3467 | 19 |
| 8 / 3. | 3.6614 | 52.3491 | 28.2654 | 1.6738 | 12.2592 | 0.2863 | 0.7604 | 0.2037 | 99.4595 | -8766 | -5502 | 148 | R-18-04_F | 11.6015 | 20 |
| 8 / 4. | 3.6339 | 51.2255 | 29.9107 | 0.581 | 13.1839 | 0.1284 | 0.1411 | 0.0426 | 98.8471 | -8795 | -5465 | 146 | R-18-04_F | 11.4475 | 21 |
| 9 / 1. | 4.7282 | 55.6261 | 27.7324 | 0.593 | 10.4211 | 0.2314 | 0.1525 | 0.0732 | 99.5578 | -15542 | -36024 | -102 | R-18-04_F | 11.3714 | 22 |
| 9 / 2. | 3.3399 | 51.3326 | 30.5562 | 0.5588 | 13.5747 | 0.1245 | 0.1303 | 0.0529 | 99.6698 | -15748 | -35988 | -101 | R-18-04_F | 11.5575 | 23 |
| 9 / 3. | 4.1895 | 52.8864 | 29.3733 | 0.7011 | 12.0271 | 0.188 | 0.1609 | 0.0632 | 99.5896 | -15799 | -35943 | -98 | R-18-04_F | 11.4769 | 24 |
| 10 / 1. | 3.4051 | 51.3011 | 30.3366 | 0.6718 | 13.326 | 0.1276 | 0.1395 | 0.0502 | 99.358 | -16051 | -35888 | -101 | R-18-04_F | 11.5221 | 25 |
| 10 / 2. | 4.3402 | 53.4597 | 28.7533 | 0.7149 | 11.6739 | 0.1726 | 0.1563 | 0.0799 | 99.3509 | -16078 | -35902 | -99 | R-18-04_F | 11.4323 | 26 |
| 10 / 3. | 4.5903 | 54.3594 | 28.2183 | 0.7642 | 11.2878 | 0.2413 | 0.1669 | 0.0823 | 99.7105 | -16094 | -35912 | -100 | R-18-04_F | 11.4582 | 27 |
| 11 / 1. | 4.7635 | 53.5738 | 27.9098 | 0.8455 | 10.7388 | 0.2634 | 0.1579 | 0.1068 | 98.3596 | -4858 | -39813 | -90 | R-18-04_F | 11.292 | 28 |
| 11 / 2. | 5.8262 | 58.3067 | 24.4532 | 1.2673 | 7.8643 | 0.6774 | 0.1213 | 0.2666 | 98.363 | -4889 | -39804 | -94 | R-18-04_F | 11.2536 | 29 |
| 12 / 1. | 5.7362 | 56.8723 | 25.8868 | 0.9652 | 8.8187 | 0.4262 | 0.1098 | 0.1431 | 98.9583 | -8513 | -40020 | -107 | R-18-04_F | 11.2693 | 30 |
| 12 / 2. | 4.7616 | 62.6805 | 14.693 | 5.5353 | 3.4255 | 2.2813 | 0.4993 | 1.6564 | 95.5329 | -8518 | -40020 | -111 | R-18-04_F | 11.323 | 31 |
| 13 / 1. | 4.4246 | 53.2035 | 28.8511 | 0.6883 | 11.6866 | 0.2001 | 0.133 | 0.0559 | 99.243 | 6847 | 37836 | 408 | R-18-10_F | 11.4183 | 32 |
| 13 / 2. | 4.3861 | 52.5237 | 28.7185 | 0.7559 | 11.6901 | 0.2326 | 0.1395 | 0.0738 | 98.5201 | 7177 | 37740 | 412 | R-18-10_F | 11.3514 | 33 |
| 13 / 3. | 2.9675 | 50.1766 | 31.5955 | 0.7061 | 14.593 | 0.1598 | 0.1383 | 0.0495 | 100.386 | 7232 | 37782 | 409 | R-18-10_F | 11.7127 | 34 |
| 13 / 4. | 5.0874 | 58.9331 | 22.7316 | 2.3649 | 7.4667 | 1.0313 | 0.1591 | 0.754 | 98.5279 | 7246 | 37796 | 410 | R-18-10_F | 11.3823 | 35 |
| 14 / 1. | 5.0378 | 54.7182 | 27.8931 | 0.9136 | 10.5119 | 0.3039 | 0.088 | 0.1021 | 99.5686 | 7485 | 37854 | 411 | R-18-10_P | 11.4181 | 36 |
| 14 / 2. | 4.9777 | 54.6916 | 28.1065 | 0.8283 | 10.6091 | 0.2629 | 0.1067 | 0.0735 | 99.6563 | 7477 | 37847 | 410 | R-18-10_P | 11.4194 | 37 |
| 15 / 1. | 5.4009 | 53.8852 | 27.5899 | 0.6563 | 10.7586 | 0.2708 | 0.132 | 0.085 | 98.7787 | 20666 | 40016 | 439 | R-18-10_P | 11.3134 | 38 |
| 15 / 2. | 4.2971 | 52.7776 | 29.2651 | 0.6887 | 11.9804 | 0.1763 | 0.1339 | 0.0586 | 99.3778 | 20513 | 39956 | 441 | R-18-10_P | 11.4486 | 39 |
| 15 / 3. | 4.5586 | 53.6074 | 28.4052 | 0.7024 | 11.4913 | 0.1869 | 0.1335 | 0.0763 | 99.1615 | 20388 | 39931 | 441 | R-18-10_P | 11.4 | 40 |
| 16 / 1. | 5.2284 | 62.0746 | 22.7455 | 1.0563 | 7.2696 | 0.5238 | 0.0882 | 0.2376 | 99.2241 | 18131 | 41055 | 439 | R-18-10_P | 11.2383 | 41 |
| 16 / 2. | 4.9581 | 54.472 | 27.9801 | 0.9352 | 10.7857 | 0.2825 | 0.0743 | 0.0753 | 99.5631 | 18131 | 41051 | 441 | R-18-10_P | 11.4333 | 42 |
| 17 / 1. | 4.5857 | 54.1394 | 28.444 | 0.6876 | 11.5381 | 0.2131 | 0.1306 | 0.0703 | 99.8086 | 10896 | 34471 | 397 | R-18-10_P | 11.4721 | 43 |
| 17 / 2. | 4.5399 | 53.703 | 28.7574 | 0.6534 | 11.4689 | 0.231 | 0.1366 | 0.0502 | 99.5403 | 10828 | 34595 | 399 | R-18-10_P | 11.435 | 44 |
| 17 / 3. | 4.5857 | 54.0507 | 28.405 | 0.6793 | 11.3528 | 0.2103 | 0.1382 | 0.0782 | 99.5003 | 10794 | 34635 | 399 | R-18-10_P | 11.4274 | 45 |
| 18 / 1. | 6.9936 | 60.1014 | 25.1049 | 0.3151 | 6.6701 | 0.5581 | 0.0156 | 0.0294 | 99.7882 | -8174 | 20412 | 308 | R-16-01_F | 11.1586 | 46 |
| 18 / 2. | 5.9296 | 57.4211 | 26.8854 | 0.4782 | 8.7176 | 0.3579 | 0.0255 | 0.0487 | 99.8641 | -8122 | 20295 | 311 | R-16-01_F | 11.2949 | 47 |
| 19 / 1. | 6.4621 | 57.8392 | 25.7527 | 0.3526 | 7.7924 | 0.3686 | 0.019 | 0.0508 | 98.6375 | -11491 | 14519 | 263 | R-16-01_P | 11.0945 | 48 |
| 19 / 2. | 5.6743 | 56.3785 | 27.0256 | 0.4781 | 9.2281 | 0.2618 | 0.0402 | 0.0528 | 99.1395 | -11592 | 14519 | 259 | R-16-01_P | 11.2414 | 49 |
| 20 / 1. | 5.7564 | 61.8685 | 15.721 | 7.8265 | 2.6521 | 1.3042 | 0.7996 | 1.7778 | 97.706 | -11885 | 13660 | 254 | R-16-01_P | 11.7058 | 50 |
| 20 / 2. | 6.7414 | 60.5444 | 24.8411 | 0.7572 | 6.7157 | 0.6369 | 0.0428 | 0.0875 | 100.367 | -11868 | 13695 | 254 | R-16-01_P | 11.2832 | 51 |
| 21 / 1. | 5.4937 | 56.8422 | 20.2618 | 4.1733 | 7.8616 | 0.7246 | 1.8016 | 0.2772 | 97.4358 | -12197 | 14176 | 258 | R-16-01_P | 11.4385 | 52 |
| 21 / 2. | 6.43 | 58.7634 | 25.2642 | 0.7801 | 7.0042 | 0.8636 | 0.0287 | 0.0845 | 99.2186 | -12213 | 14155 | 259 | R-16-01_P | 11.1937 | 53 |

## Appendix B-4: Oregon State University Electron Microprobe data: Det. Lim (ppm)

| Point | Na | Si | Al | Fe | Ca | K | Mg | Ti | O | X | Y | Z | Comment | Mean Z | Point# |
|---|---|---|---|---|---|---|---|---|---|---|---|---|---|---|---|
| 1 / 1. | 209 | 378 | 188 | 396 | 278 | | 160 | 182 | | 16997 | -5366 | 209 | TMR-18-08_Plag1 | 12.1578 | 1 |
| 1 / 2. | 229 | 383 | 198 | 409 | 283 | 214 | 155 | 182 | | 16803 | -5519 | 206 | TMR-18-08_Plag1 | 12.6848 | 2 |
| 2 / 1. | 248 | 378 | 266 | 385 | 343 | 217 | 91 | 180 | | 19133 | -10495 | 180 | TMR-18-08_Plag2 | 11.566 | 3 |
| 2 / 2. | 245 | 373 | 261 | 365 | 338 | 208 | 92 | 183 | | 18572 | -10481 | 175 | TMR-18-08_Plag2 | 11.6397 | 4 |
| 2 / 3. | 259 | 383 | 251 | 366 | 316 | 213 | 91 | 184 | | 18067 | -10608 | 176 | TMR-18-08_Plag2 | 11.5847 | 5 |
| 3 / 1. | 242 | 373 | 254 | 359 | 340 | 214 | 92 | 183 | | 20206 | -15319 | 149 | TMR-18-08_Plag3 | 11.6896 | 6 |
| 3 / 2. | 254 | 384 | 256 | 348 | 334 | 210 | 92 | 182 | | 19896 | -15359 | 146 | TMR-18-08_Plag3 | 11.6363 | 7 |
| 3 / 3. | 277 | 378 | 254 | 360 | 297 | 213 | 92 | 180 | | 19570 | -15384 | 146 | TMR-18-08_Plag3 | 11.4009 | 8 |
| 4 / 1. | 268 | 373 | 247 | 347 | 317 | 214 | 89 | 179 | | 12366 | -25656 | 57 | TMR-18-08_Plag4 | 11.4926 | 9 |
| 4 / 2. | 288 | 369 | 241 | 359 | 310 | 211 | 90 | 177 | | 12518 | -25806 | 57 | TMR-18-08_Plag4 | 11.3491 | 10 |
| 5 / 1. | 284 | 377 | 251 | 356 | 327 | 216 | 90 | 181 | | 12989 | -25687 | 59 | TMR-18-08_Plag5 | 11.3078 | 11 |
| 5 / 2. | 273 | 377 | 254 | 351 | 318 | 214 | 90 | 181 | | 13001 | -25699 | 59 | TMR-18-08_Plag5 | 11.4972 | 12 |
| 5 / 3. | 301 | 376 | 248 | 355 | 310 | 217 | 91 | 177 | | 13009 | -25704 | 57 | TMR-18-08_Plag5 | 11.3364 | 13 |
| 6 / 1. | 263 | 367 | 250 | 355 | 333 | 210 | 88 | 178 | | 6471 | -38900 | -48 | TMR-18-08_Plag6 | 11.1954 | 14 |
| 6 / 2. | 292 | 368 | 245 | 353 | 297 | 209 | 88 | 177 | | 6472 | -38908 | -45 | TMR-18-08_Plag6 | 11.2345 | 15 |
| 7 / 1. | 244 | 368 | 259 | 368 | 333 | 220 | 92 | 184 | | -23495 | -8050 | 80 | TMR-18-04_Plag1 | 11.7041 | 16 |
| 7 / 2. | 282 | 373 | 253 | 356 | 308 | 208 | 91 | 183 | | -23345 | -8188 | 79 | TMR-18-04_Plag1 | 11.4649 | 17 |
| 8 / 1. | 241 | 381 | 265 | 348 | 302 | 212 | 93 | 183 | | -8605 | -5855 | 142 | TMR-18-04_Plag2 | 11.6144 | 18 |
| 8 / 2. | 282 | 376 | 253 | 357 | 325 | 214 | 92 | 182 | | -8802 | -5655 | 148 | TMR-18-04_Plag2 | 11.3467 | 19 |
| 8 / 3. | 270 | 384 | 250 | 352 | 331 | 209 | 93 | 181 | | -8766 | -5502 | 148 | TMR-18-04_Plag2 | 11.6015 | 20 |
| 8 / 4. | 272 | 383 | 257 | 361 | 316 | 216 | 91 | 183 | | -8795 | -5465 | 146 | TMR-18-04_Plag2 | 11.4475 | 21 |
| 9 / 1. | 295 | 383 | 254 | 343 | 305 | 215 | 91 | 181 | | -15542 | -36024 | -102 | TMR-18-04_Plag3 | 11.3714 | 22 |
| 9 / 2. | 267 | 381 | 258 | 358 | 333 | 213 | 92 | 182 | | -15748 | -35988 | -101 | TMR-18-04_Plag3 | 11.5575 | 23 |
| 9 / 3. | 270 | 382 | 263 | 347 | 319 | 214 | 90 | 182 | | -15799 | -35943 | -98 | TMR-18-04_Plag3 | 11.4769 | 24 |
| 10 / 1. | 267 | 369 | 251 | 345 | 332 | 213 | 90 | 180 | | -16051 | -35888 | -101 | TMR-18-04_Plag4 | 11.5221 | 25 |
| 10 / 2. | 283 | 380 | 249 | 360 | 339 | 214 | 90 | 177 | | -16078 | -35902 | -99 | TMR-18-04_Plag4 | 11.4323 | 26 |
| 10 / 3. | 275 | 376 | 246 | 354 | 315 | 215 | 88 | 176 | | -16094 | -35912 | -100 | TMR-18-04_Plag4 | 11.4582 | 27 |
| 11 / 1. | 291 | 371 | 252 | 352 | 296 | 211 | 91 | 179 | | -4858 | -39813 | -90 | TMR-18-04_Plag5 | 11.292 | 28 |
| 11 / 2. | 301 | 388 | 247 | 357 | 306 | 215 | 90 | 180 | | -4889 | -39804 | -94 | TMR-18-04_Plag6 | 11.2536 | 29 |
| 12 / 1. | 302 | 384 | 249 | 352 | 302 | 215 | 90 | 179 | | -8513 | -40020 | -107 | TMR-18-04_Plag6 | 11.2693 | 30 |
| 12 / 2. | 295 | 402 | 224 | 385 | 283 | 238 | 92 | 188 | | -8518 | -40020 | -111 | TMR-18-04_Plag6 | 11.323 | 31 |
| 13 / 1. | 284 | 394 | 252 | 359 | 322 | 211 | 91 | 180 | | 6847 | 37836 | 408 | TMR-18-10_Plag1 | 11.4183 | 32 |
| 13 / 2. | 280 | 380 | 252 | 362 | 310 | 207 | 90 | 180 | | 7177 | 37740 | 412 | TMR-18-10_Plag1 | 11.3514 | 33 |
| 13 / 3. | 263 | 381 | 253 | 345 | 343 | 206 | 91 | 182 | | 7232 | 37782 | 409 | TMR-18-10_Plag1 | 11.7127 | 34 |
| 13 / 4. | 293 | 383 | 241 | 356 | 328 | 222 | 91 | 183 | | 7246 | 37796 | 410 | TMR-18-10_Plag1 | 11.3823 | 35 |
| 14 / 1. | 294 | 370 | 245 | 358 | 318 | 210 | 91 | 176 | | 7485 | 37854 | 411 | TMR-18-10_Plag2 | 11.4181 | 36 |
| 14 / 2. | 284 | 383 | 246 | 346 | 320 | 215 | 89 | 176 | | 7477 | 37847 | 410 | TMR-18-10_Plag2 | 11.4194 | 37 |
| 15 / 1. | 295 | 375 | 239 | 355 | 339 | 208 | 89 | 178 | | 20666 | 40016 | 439 | TMR-18-10_Plag3 | 11.3134 | 38 |
| 15 / 2. | 277 | 372 | 246 | 341 | 319 | 217 | 89 | 179 | | 20513 | 39956 | 441 | TMR-18-10_Plag3 | 11.4486 | 39 |
| 15 / 3. | 284 | 373 | 249 | 343 | 296 | 212 | 91 | 177 | | 20388 | 39931 | 441 | TMR-18-10_Plag3 | 11.4 | 40 |
| 16 / 1. | 299 | 387 | 233 | 339 | 335 | 214 | 90 | 180 | | 18131 | 41055 | 439 | TMR-18-10_Plag4 | 11.2383 | 41 |
| 16 / 2. | 295 | 381 | 254 | 362 | 300 | 216 | 92 | 183 | | 18131 | 41051 | 441 | TMR-18-10_Plag4 | 11.4333 | 42 |
| 17 / 1. | 280 | 370 | 243 | 349 | 310 | 211 | 90 | 177 | | 10896 | 34471 | 397 | TMR-18-10_Plag5 | 11.4721 | 43 |
| 17 / 2. | 287 | 377 | 245 | 346 | 301 | 212 | 89 | 179 | | 10828 | 34595 | 399 | TMR-18-10_Plag5 | 11.435 | 44 |
| 17 / 3. | 281 | 370 | 249 | 347 | 318 | 215 | 89 | 178 | | 10794 | 34635 | 399 | TMR-18-10_Plag5 | 11.4274 | 45 |
| 18 / 1. | 317 | 382 | 239 | 346 | 310 | 219 | 89 | 180 | | -8174 | 20412 | 308 | TMR-16-01_Plag1 | 11.1586 | 46 |
| 18 / 2. | 313 | 376 | 253 | 339 | 325 | 216 | 90 | 180 | | -8122 | 20295 | 311 | TMR-16-01_Plag1 | 11.2949 | 47 |
| 19 / 1. | 309 | 378 | 241 | 335 | 307 | 210 | 88 | 174 | | -11491 | 14519 | 263 | TMR-16-01_Plag2 | 11.0945 | 48 |
| 19 / 2. | 295 | 381 | 244 | 362 | 308 | 206 | 90 | 178 | | -11592 | 14519 | 259 | TMR-16-01_Plag2 | 11.2414 | 49 |
| 20 / 1. | 315 | 388 | 218 | 385 | 296 | 228 | 90 | 186 | | -11885 | 13660 | 254 | TMR-16-01_Plag3 | 11.7058 | 50 |
| 20 / 2. | 316 | 381 | 239 | 351 | 321 | 217 | 88 | 176 | | -11868 | 13695 | 254 | TMR-16-01_Plag3 | 11.2832 | 51 |
| 21 / 1. | 303 | 371 | 225 | 376 | 321 | 218 | 97 | 181 | | -12197 | 14176 | 258 | TMR-16-01_Plag4 | 11.4385 | 52 |
| 21 / 2. | 312 | 386 | 239 | 372 | 289 | 217 | 88 | 180 | | -12213 | 14155 | 259 | TMR-16-01_Plag4 | 11.1937 | 53 |

Appendix B-5: Oregon State University Electron Microprobe data: LABR standard (weight %)

| Point | Na | Si | Al | Fe | Ca | K | Mg | Ti | O | Total | X | Y | Z | Comment | Mean Z |
|---|---|---|---|---|---|---|---|---|---|---|---|---|---|---|---|
| 1 / 1 . | 2.5553 | 23.7898 | 16.3997 | 0.3463 | 9.7144 | 0.0986 | 0.0836 | 0.028 | 46.6532 | 99.6689 | -9528 | 27462 | 324 | LABR | 11.5437 |
| 1 / 2 . | 2.593 | 24.2102 | 16.5787 | 0.352 | 9.8099 | 0.0872 | 0.0829 | 0.0332 | 47.3449 | 101.0918 | -9506 | 27462 | 324 | LABR | 11.7048 |
| 1 / 3 . | 2.549 | 24.0735 | 16.3665 | 0.3663 | 9.7692 | 0.0861 | 0.0845 | 0.0341 | 46.9745 | 100.3037 | -9505 | 27480 | 324 | LABR | 11.6194 |
| 1 / 4 . | 2.5454 | 23.9177 | 16.3278 | 0.3562 | 9.8278 | 0.0859 | 0.0801 | 0.03 | 46.7761 | 99.9471 | -9493 | 27497 | 324 | LABR | 11.5839 |
| 1 / 5 . | 2.5272 | 24.208 | 16.2832 | 0.3158 | 9.6687 | 0.0862 | 0.0805 | 0.025 | 46.9827 | 100.1773 | -9476 | 27507 | 324 | LABR | 11.5899 |

## Appendix C: Sample Locations

| Sample ID | Latitude | Longitude | Elevation (ft) |
|---|---|---|---|
| TMR-16-01 | 44.090049 | -121.63217 | 6703 |
| TMR-16-02 | 44.089717 | -121.63304 | 7146 |
| TMR-16-03 | 44.089216 | -121.63400 | 7278 |
| TMR-18-03 | 44.091360 | -121.63790 | 7579 |
| TMR-18-04 | 44.090660 | -121.63733 | 7483 |
| TMR-18-05 | 44.094900 | -121.63371 | 6778 |
| TMR-18-06 | 44.100360 | -121.65291 | 7378 |
| TMR-18-07 | 44.099860 | -121.65322 | 7250 |
| TMR-18-08 | 44.100520 | -121.65323 | 7437 |
| TMR-18-09 | 44.100610 | -121.65377 | 7500 |
| TMR-18-10 | 44.100260 | -121.65546 | 7532 |